Article

Developmental Cell

EPLINα controls integrin recycling from Rab21 endosomes to drive breast cancer cell migration

Graphical abstract

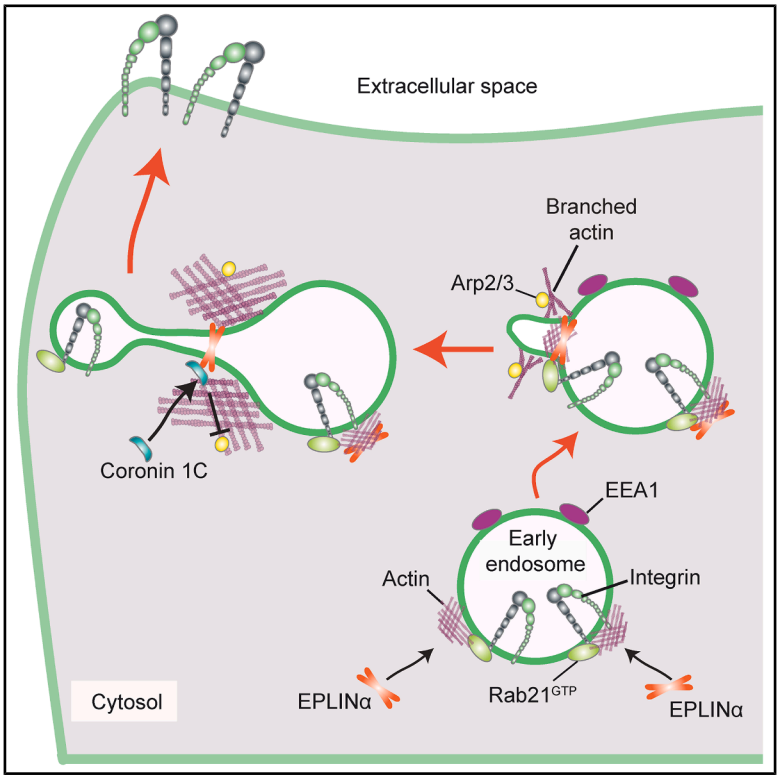

Highlights

- EPLINα mediates integrin recycling from Rab21-positive early endosomes
- EPLINα-actin-binding function is required for integrin recycling and cell migration
- EPLINα is the predominant isoform in mesenchymal-like breast cancer cells
- Shared and isoform-specific EPLIN interactors identified using BioID

Authors

Niklas Z. Jäntti, Paulina Moreno-Layseca, Megan R. Chastney, ..., Leticia Oliveira-Ferrer, Stefan Veltel, Johanna Ivaska

Correspondence

pmolay@utu.fi (P.M.-L.), joivaska@utu.fi (J.I.)

In brief

Jäntti et al. report that EPLINα plays an isoform-specific role in actin-dependent recycling of integrins, promoting breast cancer cell migration. They identified shared and distinct interactors of EPLINα and EPLINβ and found that triple-negative breast tumors predominantly express EPLINα.

Jäntti et al., 2025, Developmental Cell *60*, 1–16
December 15, 2025
https://doi.org/10.1016/j.devcel.2025.06.025

CellPress

Developmental Cell

CellPress
OPEN ACCESS

Article

EPLINα controls integrin recycling from Rab21 endosomes to drive breast cancer cell migration

Niklas Z. Jäntti,[1] Paulina Moreno-Layseca,[1,*] Megan R. Chastney,[1] Michal Dibus,[1] James R.W. Conway,[1,8] Veli-Matti Leppänen,[1] Hellyeh Hamidi,[1] Kathrin Eylmann,[2] Leticia Oliveira-Ferrer,[2] Stefan Veltel,[3] and Johanna Ivaska[1,4,5,6,7,9,*]

[1]Turku Bioscience Centre, University of Turku and Åbo Akademi University, 20520 Turku, Finland
[2]University Medical Center Hamburg-Eppendorf (UKE), 20251 Hamburg, Germany
[3]Hochschule Bremen, City University of Applied Sciences, 28199 Bremen, Germany
[4]Department of Life Technologies, University of Turku, 20520 Turku, Finland
[5]InFLAMES Research Flagship, University of Turku, 20014 Turku, Finland
[6]Western Finnish Cancer Center (FICAN West), University of Turku, 20520 Turku, Finland
[7]Foundation for the Finnish Cancer Institute, Tukholmankatu 8, 00014 Helsinki, Finland
[8]Present address: Department of Biochemistry and Developmental Biology, Faculty of Medicine, University of Helsinki, Helsinki, Finland
[9]Lead contact
*Correspondence: pmolay@utu.fi (P.M.-L.), joivaska@utu.fi (J.I.)
https://doi.org/10.1016/j.devcel.2025.06.025

SUMMARY

Epithelial protein lost in neoplasm (EPLIN), an actin-binding protein, has been described as both a tumor promoter and tumor suppressor in different cancers. The roles of EPLIN isoforms (α/β) remain largely unknown and could explain these opposing views. We observed distinct EPLIN isoform localization in breast cancer cells; EPLINα is recruited to actin in plasma membrane ruffles and endosomes, while EPLINβ resides on stress fibers. EPLINα localizes to early endosomes in an actin-dependent manner, where it interacts with Rab21, an established regulator of β1-integrin endosomal trafficking. This supports β1-integrin recycling and cell migration. Using proximity biotinylation (BioID), we identified coronin 1C as an EPLIN-proximal protein, which also localizes at Rab21-containing endosomes and controls integrin recycling downstream of EPLINα. EPLINα expression was linked to increased breast cancer cell motility, and a high EPLINα-to-EPLINβ ratio correlated with a mesenchymal phenotype in patient samples. Our work identifies previously unknown EPLIN-isoform-specific functions relevant to breast cancer and beyond.

INTRODUCTION

Epithelial protein lost in neoplasm (EPLIN) is an LIM-domain-containing, actin-binding protein. Since its discovery two decades ago, it has been linked to the regulation of cytoskeletal dynamics by bundling and crosslinking actin and implicated in cancer progression.[1–3] EPLIN is encoded by the LIM domain and actin-binding protein 1 (*LIMA1*) gene, but has two isoforms, α and β, generated by alternative promoters.[4] The isoforms are identical, except for the presence of an additional 160 amino acids at the N terminus of EPLINβ (Figure 1A).

As its name suggests, EPLIN has been described as a potential tumor suppressor due to its loss in a range of epithelial tumors.[1,5] However, EPLIN has been shown to be upregulated in head and neck tumors and hepatocellular carcinoma, suggesting a pro-tumorigenic role.[6–8] These contradictory roles could be due to distinct or even opposing functions of its isoforms.

In addition to cytoskeletal functions, EPLIN is a structural component of adherens junctions, linking filamentous actin (F-actin) to the cadherin-catenin complex,[9] and participates in the accumulation of mitotic regulatory proteins at the cleavage furrow,[10] where it is regulated by kinases and phosphatases, such as ERK[11] and CDC14A.[12] EPLIN also binds to the endocytic molecule caveolin[13] and localizes to integrin adhesions in a PINCH-dependent manner in keratinocytes.[14] PINCH is a part of the ILK-PINCH-parvin (IPP) complex, which recruits molecules to integrin adhesion sites.[15] Furthermore, EPLIN controls cholesterol absorption in the gut by aiding the recycling of NPC1L1, a transmembrane receptor expressed in the gastrointestinal tract.[16] Despite these discoveries linking EPLIN to several important processes, the underlying molecular mechanisms, and especially the specific roles of each EPLIN isoform, have remained largely unexplored.

The endosomal transport of integrins, which allows internalization and delivery of receptors to and from the plasma membrane, is required for adequate integrin adhesion formation and disassembly during cell migration.[17,18] We have previously identified the actin-binding protein Swiprosin-1 (Swip1; EFHD2) as an interactor of the small GTPase Rab21,[19] and as an essential cargo adaptor for endocytosis of active β1-integrins via the CLIC/GEEC pathway.[20] Elevated integrin endocytosis by the Rab21-Swip1 axis increases cell migration and invasion and correlates

Please cite this article in press as: Jäntti et al., EPLINα controls integrin recycling from Rab21 endosomes to drive breast cancer cell migration, Developmental Cell (2025), https://doi.org/10.1016/j.devcel.2025.06.025

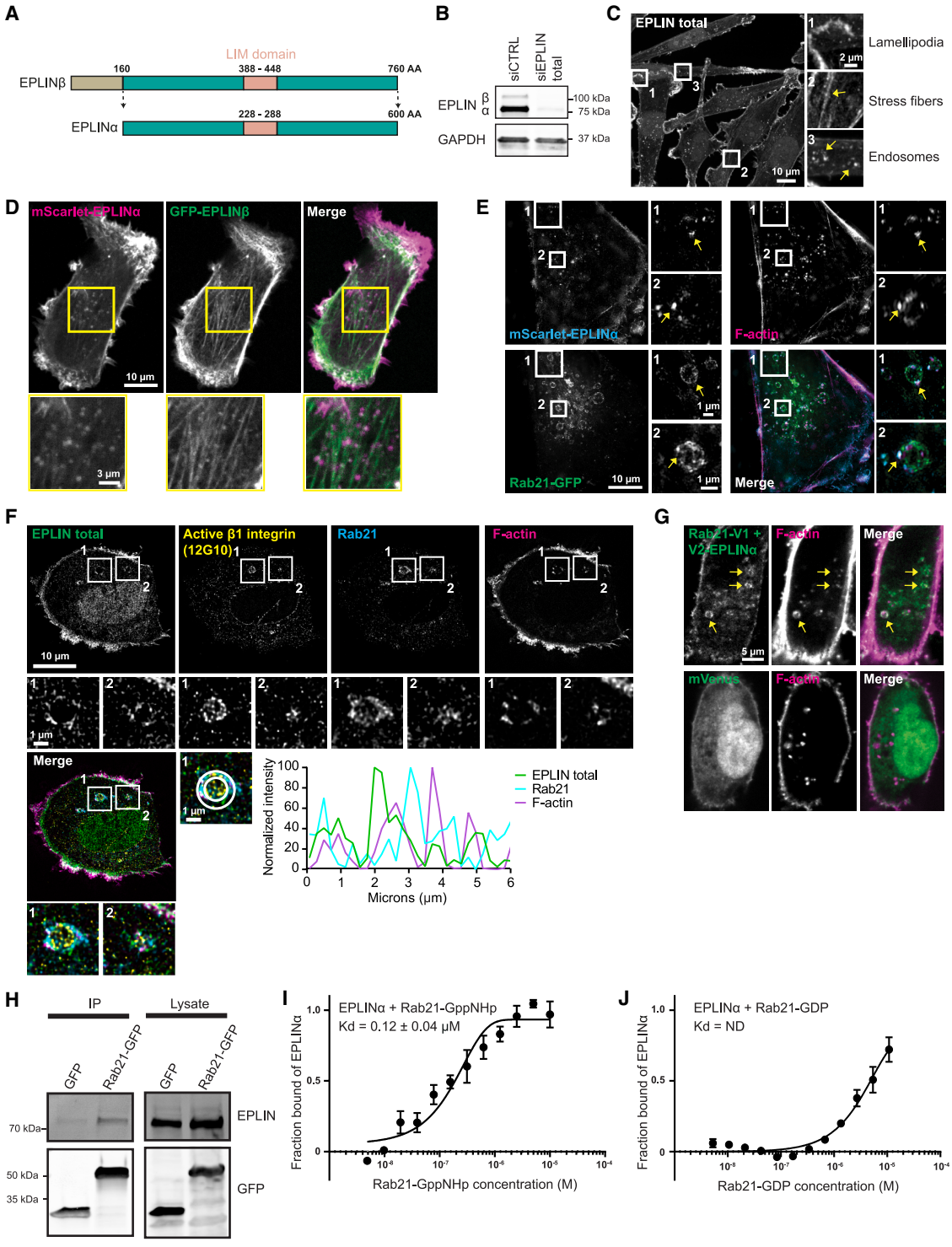

Figure 1. EPLINα interacts directly with GTP-bound Rab21 at endosomal compartments

(A) Schematic representation of EPLIN isoforms, generated by the authors.

(B) Representative immunoblot showing expression of EPLIN isoforms in MDA-MB-231 cells.

(C) Representative MDA-MB-231 cells immunostained with antibodies that detect both EPLIN isoforms (EPLIN total). Insets highlight the different localizations of EPLIN: actin-rich protrusions (inset 1), stress fibers (inset 2), and endosomes (inset 3). Arrows point to structures of interest.

(D) MDA-MB-231 live cells overexpressing mScarlet-EPLINα and GFP-EPLINβ. The yellow square highlights a region of interest (ROI) showing localization of mScarlet-EPLINα primarily on endosomes and GFP-EPLINβ primarily on stress fibers.

(legend continued on next page)

Please cite this article in press as: Jäntti et al., EPLINα controls integrin recycling from Rab21 endosomes to drive breast cancer cell migration, Developmental Cell (2025), https://doi.org/10.1016/j.devcel.2025.06.025

with poor prognosis in triple-negative breast cancer.[19] However, the mechanism regulating the recycling of the Rab21-Swip1 endocytosed integrins has not been previously investigated.

Here, we identify EPLINα as a direct interactor of Rab21 at early endosomes. We find that EPLINα controls the recycling of integrins from these endosomes in an actin-dependent manner. EPLINα resides on Rab21-positive early endosomes at localized puncta together with F-actin and coronin 1C (CORO1C), from where tubules are generated. Our study shows that EPLINα promotes integrin transport to drive migration of cancer cells, identifies isoform-specific proximity interactors, and shows that the balance between EPLIN isoforms in cells correlates with their migratory potential.

RESULTS

EPLINα interacts directly with Rab21 at endosomal compartments

Although our recent work detailed the mechanism of Rab21-mediated recruitment and endocytosis of active integrins, the key players regulating integrin recycling from these compartments remained unknown. EPLIN was identified as a putative Rab21 interactor in our previous screen in MDA-MB-231 cells.[19] These cells express both EPLIN isoforms, EPLINα and EPLINβ, with EPLINα being the predominant isoform (Figures 1A and 1B). Immunofluorescence staining of EPLIN with an antibody recognizing both isoforms (referred to as total EPLIN) showed the endogenous protein localizing to actin-rich protrusions and stress fibers, but also on intracellular actin-positive endosomal-like structures (Figure 1C).

Co-expression of both EPLIN isoforms revealed shared and distinct subcellular localizations (Figure 1D). Both isoforms localized to the actin cortex and lamellipodia, as previously reported.[21,22] However, EPLINβ was strongly enriched on actin stress fibers, while EPLINα was present in endosomal-looking structures. Super-resolution structured illumination microscopy (SIM) revealed that EPLINα localized to Rab21-positive endosomes in a punctate distribution around the endosome, which mirrored the localization of endosomal F-actin (Figure 1E). To validate our observation, we performed high-resolution imaging to visualize endogenous EPLIN and Rab21 using a knockin cell line where endogenous Rab21 was tagged with mScarlet. We observed both endogenous EPLIN and Rab21 in endosomes containing active β1-integrin, a known cargo for Rab21-positive endosomes[19,20,23] (Figure 1F). Line scan analysis showed that EPLIN and F-actin share the same punctate distribution around the endosome, while Rab21 is in close vicinity to EPLIN, with partial overlap. Bimolecular fluorescence complementation (BiFC) experiments[24] showed a positive interaction between the Rab21-EPLINα pair on endosomes decorated with F-actin (Figure 1G). This interaction was absent in the mVenus control. Furthermore, endogenous EPLIN co-precipitated with GFP-tagged Rab21, but not the GFP-only control (Figure 1H). In addition, microscale thermophoresis (MST) experiments demonstrated direct binding between guanosine triphosphate (GTP)-analog-loaded recombinant Rab21 and purified recombinant GST-EPLINα with micromolar affinity (Figures 1I, S1A, and S1B), which was only weakly observed for guanosine diphosphate (GDP)-loaded Rab21 (Figure 1J). Together, these results indicate that EPLINα and GTP-loaded Rab21 interact directly and localize at endosomes containing active β1-integrin, where EPLINα co-localizes with F-actin.

EPLINα controls the recycling of active integrins from early endosomes

Since Rab21 plays a key role in integrin traffic, we asked whether EPLINα could be involved in this function as well. To answer this question, we performed a fluorescence-microscopy-based β1-integrin internalization assay to measure the internalization of cell-surface-labeled active β1-integrins. Since EPLINβ is also expressed in MDA-MB-231 cells, we tested its potential contribution to integrin traffic regulation. Silencing of both EPLIN isoforms (EPLIN total) resulted in an increase of intracellular cell surface-labeled active β1-integrin after 15 min of internalization. Conversely, silencing EPLINβ alone had no significant effect, suggesting that the EPLINα isoform specifically regulates active β1-integrin trafficking (Figure 2A).

This internalization assay was performed in the presence of serum, where constant integrin endocytosis is balanced with receptor recycling back to the plasma membrane.[25] Thus, increased accumulation of active β1-integrin inside the cell could be caused by either enhanced receptor internalization or a defect in recycling. To study this in more detail, we performed another set of trafficking experiments, incorporating the recycling step by utilizing a previously established fluorescence-quenching-based method.[25] In this case, integrin internalization was first performed in the absence of serum to prevent constitutive recycling. Under this condition, equivalent levels of endocytosed integrin were detected in the control and total EPLIN-silenced conditions, discounting EPLIN as a regulator of integrin

(E) Representative SIM image of MDA-MB-231 cell expressing mScarlet-EPLINα and Rab21-GFP and labeled with Phalloidin-Atto 647N. Arrows point to EPLINα overlap with F-actin in Rab21-containing endosomes.
(F) Representative deconvolved image of maximum-intensity projection of two slices from the middle of an MDA-MB-231 cell expressing endogenously tagged Rab21-mScarlet, immunostained for EPLIN total and active β1-integrin (12G10), and labeled with Phalloidin-Atto 647N. Insets (1 and 2) show Rab21-positive endosomes containing active β1-integrin, EPLIN, and F-actin. Histogram shows fluorescence intensity at the periphery of the endosome (indicated with a circle).
(G) Representative confocal microscopy BiFC images of MDA-MB-231 cells expressing the BiFC constructs Rab21-V1 and EPLINα-V2 or Venus alone as a control in cells stained with Phalloidin-Atto 647N. Arrows indicate BiFC colocalizing with F-actin.
(H) Representative immunoblots of GFP-Trap pull-downs from MDA-MB-231 cells transfected with the indicated constructs and probed for GFP and endogenous EPLIN.
(I and J) Binding of recombinant EPLINα to fluorescently labeled (I) non-hydrolysable GTP analog (GppNHp)-loaded or (J) GDP-loaded recombinant Rab21 in microscale thermophoresis. Plot shows mean fraction bound and standard error of the mean from three (I) or four (J) independent experiments. ND, not determined.
(B–H) Representative from three independent experiments.
See also Figure S1.

Please cite this article in press as: Jäntti et al., EPLINα controls integrin recycling from Rab21 endosomes to drive breast cancer cell migration, Developmental Cell (2025), https://doi.org/10.1016/j.devcel.2025.06.025

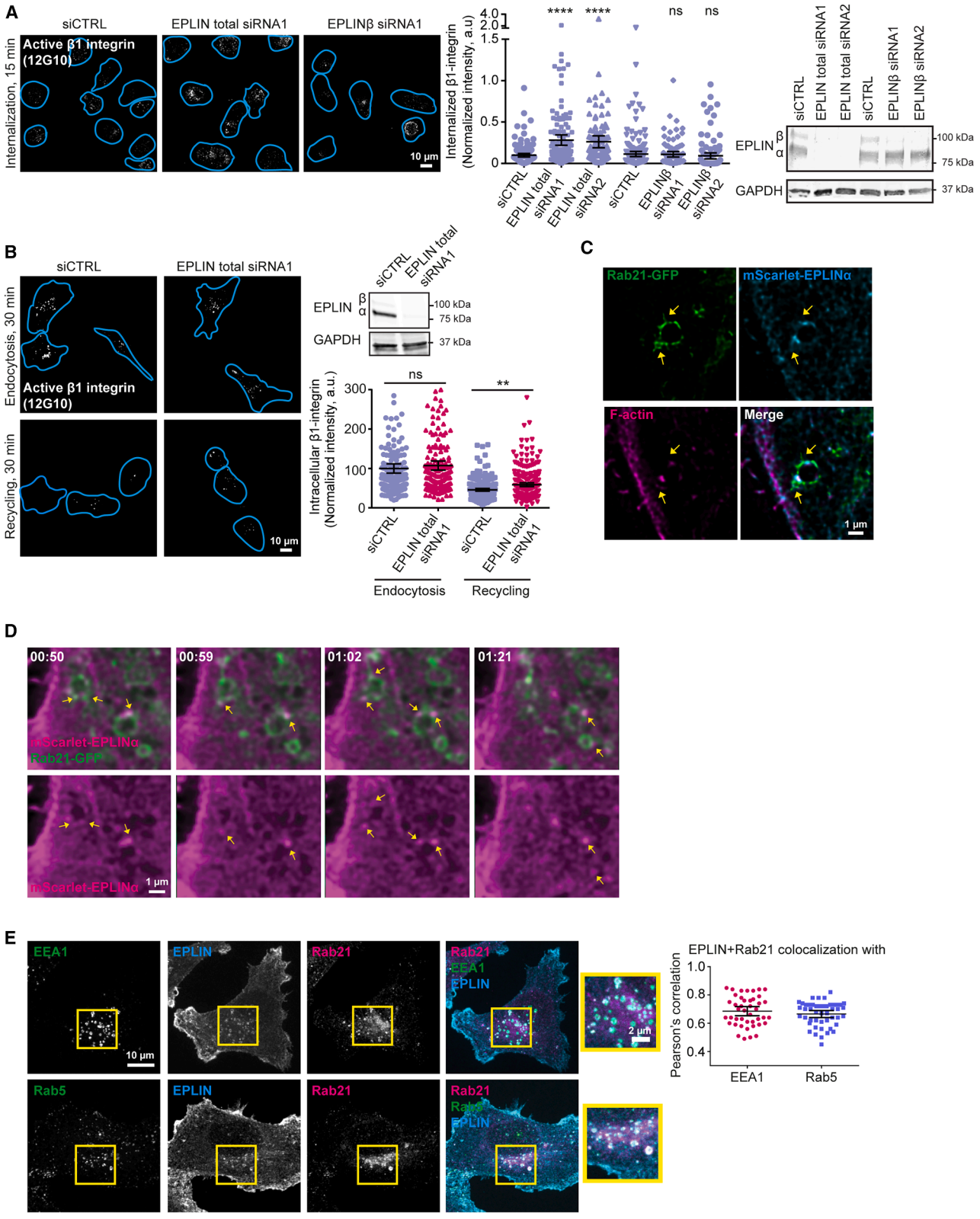

Figure 2. EPLINα controls the recycling of active integrins from early endosomes

(A) Representative micrographs of active β1-integrin (12G10) internalization at 15 min in control (siCTRL)- and EPLIN-silenced MDA-MB-231 cells (blue lines show the outlines of the cells defined by Phalloidin-Atto 647N labeling). A representative immunoblot validating EPLIN silencing is shown (right), along with

(legend continued on next page)

Please cite this article in press as: Jäntti et al., EPLINα controls integrin recycling from Rab21 endosomes to drive breast cancer cell migration, Developmental Cell (2025), https://doi.org/10.1016/j.devcel.2025.06.025

internalization. Next, we triggered receptor recycling by adding serum and quantified the remaining signal inside the cell. More integrin signal was detected in the EPLIN-silenced cells after this step, indicating a defect in recycling (Figure 2B). Importantly, EPLINβ expression did not rescue the recycling defect observed in EPLIN-silenced cells (Figure S2), ruling out a potential contribution from the β isoform and suggesting that the EPLINα isoform alone is contributing to integrin recycling.

Cargo recycling from endosomes requires the formation of tubules destined for the plasma membrane.[26] Deconvolved high-resolution images of mScarlet-EPLINα and Rab21-GFP revealed Rab21- and EPLINα-positive tubules emanating from the endosomes (Figure 2C). Live-cell imaging further validated these findings, showing tubule formation from Rab21-positive endosomes originating at EPLINα puncta (Figure 2D; Video S1).

Building on this finding, we observed that EPLINα resides in Rab21-containing endosomes at the perinuclear region, but not in the smaller Rab21-positive puncta at the cell periphery (Figures 1F and 2E), which mainly comprise the early endocytic CLICs.[19] Moreover, Rab21 has been shown to localize to EEA1 and Rab5 early endosomes,[20,23,27] which are bigger than CLICs, and serve as key sites for the fast recycling of cargo.[17,28] Immunofluorescent staining for early endosomal markers showed that EPLIN- and Rab21-positive endosomes had a high degree of co-localization with both Rab5 and EEA1 (Figure 2E). Together, these results indicate that EPLINα localizes to Rab21-positive early endosomes to mediate the recycling of active β1-integrin.

The actin-binding function of EPLINα is required for endosomal localization and integrin recycling

Next, we investigated whether Rab21 was required for the endosomal localization of EPLINα. Surprisingly, Rab21 silencing did not affect the endosomal localization of EPLINα (Figure S3), suggesting that EPLINα could be recruited to the endosomes via F-actin. In order to assess this hypothesis, we aimed to perturb its actin-binding function. EPLINα harbors at least two actin-binding sites within the N-terminal and C-terminal domains flanking the centrally located LIM domain[21]; however, their precise location remains unknown. Analysis of the primary sequence of EPLINα using the eukaryotic linear motif (ELM) resource (http://elm.eu.org/) suggested a WH2 actin-binding motif at the C-terminal part of the protein as one of the actin-binding sites. In addition, the structural prediction by AlphaFold3[29] suggested that there is a short α helix (107–121) in the N-terminal region that could contribute to actin binding (Figure 3A). Therefore, we created three mutants of EPLINα lacking either the short N-terminal helix (ΔNHX, residues 107–121), the C-terminal WH2 motif (ΔWH2, residues 565–581), or both (ΔΔ) and used them to pull down endogenous actin (Figure 3B). While each of the single mutants showed a partial decrease in actin binding, actin binding was almost completely abolished in the case of the double mutant (Figures 3C and 3D). Moreover, the association between EPLINα wild type (WT) and ARPC1B, a subunit of the ARP2/3 complex, suggests that both of the identified actin-binding sites bind fibrillar actin (Figures 3C and 3E).

Live imaging of MDA-MB-231 cells co-transfected with mScarlet-EPLINα-WT and GFP-EPLINα-ΔΔ revealed decreased EPLINα-ΔΔ localization to endosomal structures (Figure 3F; Video S2). We then tested whether the loss of actin binding would affect the ability of EPLINα to promote active β1-integrin recycling. Silencing of total EPLIN reduced the recycling of active β1-integrin, in line with Figure 2B. Re-expression of small interfering RNA (siRNA)-resistant mScarlet-EPLINα-WT was sufficient to fully rescue the active β1-integrin recycling back to control levels, while expression of mScarlet-EPLINα-ΔΔ was unable to rescue the recycling defect (Figure 3G). Thus, EPLINα requires its actin-binding function to promote recycling of active β1-integrin.

BioID identifies proximity interactors for EPLINα and EPLINβ

Next, we performed proximity biotinylation (BioID) coupled to mass spectrometry to identify proximity interactors for EPLINα and EPLINβ. BirA*-tagged EPLINα (BirA*-EPLINα), EPLINβ (BirA*-EPLINβ), and BirA*-only control (BirA*) were stably expressed in two breast cancer cell lines, MDA-MB-231 and HCC1937. In both cell lines, the subcellular localization of BirA*-EPLINα and BirA*-EPLINβ was similar to endogenous/fluorescently tagged constructs, while the BirA*-only control showed no specific subcellular distribution and had lower expression levels (Figures 4A and S4A). To identify EPLIN proximity interactors, biotinylated proteins were isolated and analyzed using mass spectrometry, and SAINTexpress[31] was used to identify high-confidence bait-prey interactions. A total of 91 proteins (between 54 and 57 per bait) were identified as proximity interactors (BFDR $\leq$ 0.05) of BirA*-EPLINα and BirA*-EPLINβ across both cell lines

quantification of the levels of internalized β1-integrin (middle). siCTRL, *n* = 142 cells; EPLIN total siRNA1, *n* = 120 cells; EPLIN total siRNA2, *n* = 102; siCTRL, *n* = 177; EPLINβ siRNA1, *n* = 95; EPLINβ siRNA2, *n* = 107, from left to right.

(B) Representative micrographs of internalized active β1-integrin after 30 min of endocytosis and after 30 min of recycling in the presence of a quencher. Representative immunoblot to validate EPLIN silencing and quantification of the levels of internalized β1-integrin are shown. For endocytosis, siCTRL, *n* =170 and EPLIN siRNA1, *n* = 189 cells; for recycling, siCTRL, *n* = 198 and EPLIN siRNA1, *n* = 246 cells.

(C) Deconvolved airyscan images of MDA-MB-231 cells expressing Rab21-GFP and mScarlet-EPLINα and labeled with Phalloidin-Atto 647N. Arrows point to tubular structures emerging from the endosome.

(D) Deconvolved confocal images of live MDA-MB-231 cells expressing Rab21-GFP and mScarlet-EPLINα. Arrows point to EPLIN puncta in Rab21-containing endosomes, from which tubules are generated.

(E) Representative images of MDA-MB-231 cells expressing endogenously tagged Rab21-mScarlet and immunostained for EPLIN and either EEA1 or Rab5. Insets show endosomes where Rab21 and EPLIN overlap with either EEA1 or Rab5. Colocalization of Rab21- and EPLIN-positive endosomes with either EEA1 or Rab5 per cell was quantified using Pearson's coefficient. EEA1, *n* = 43 and Rab5, *n* = 47 cells.

For (A), (B), and (E), scatter dot plots show data as the mean ± 95% confidence interval (CI). Statistical significance was assessed using Mann-Whitney test (A) and Kruskal-Wallis one-way ANOVA and Dunn's post hoc test (B). $^{**}p < 0.003$, $^{****}p < 0.0001$; ns, not significant; a.u., arbitrary units. All analyzed data and representative images are from three independent experiments.

See also Figure S2 and Video S1.

Please cite this article in press as: Jäntti et al., EPLINα controls integrin recycling from Rab21 endosomes to drive breast cancer cell migration, Developmental Cell (2025), https://doi.org/10.1016/j.devcel.2025.06.025

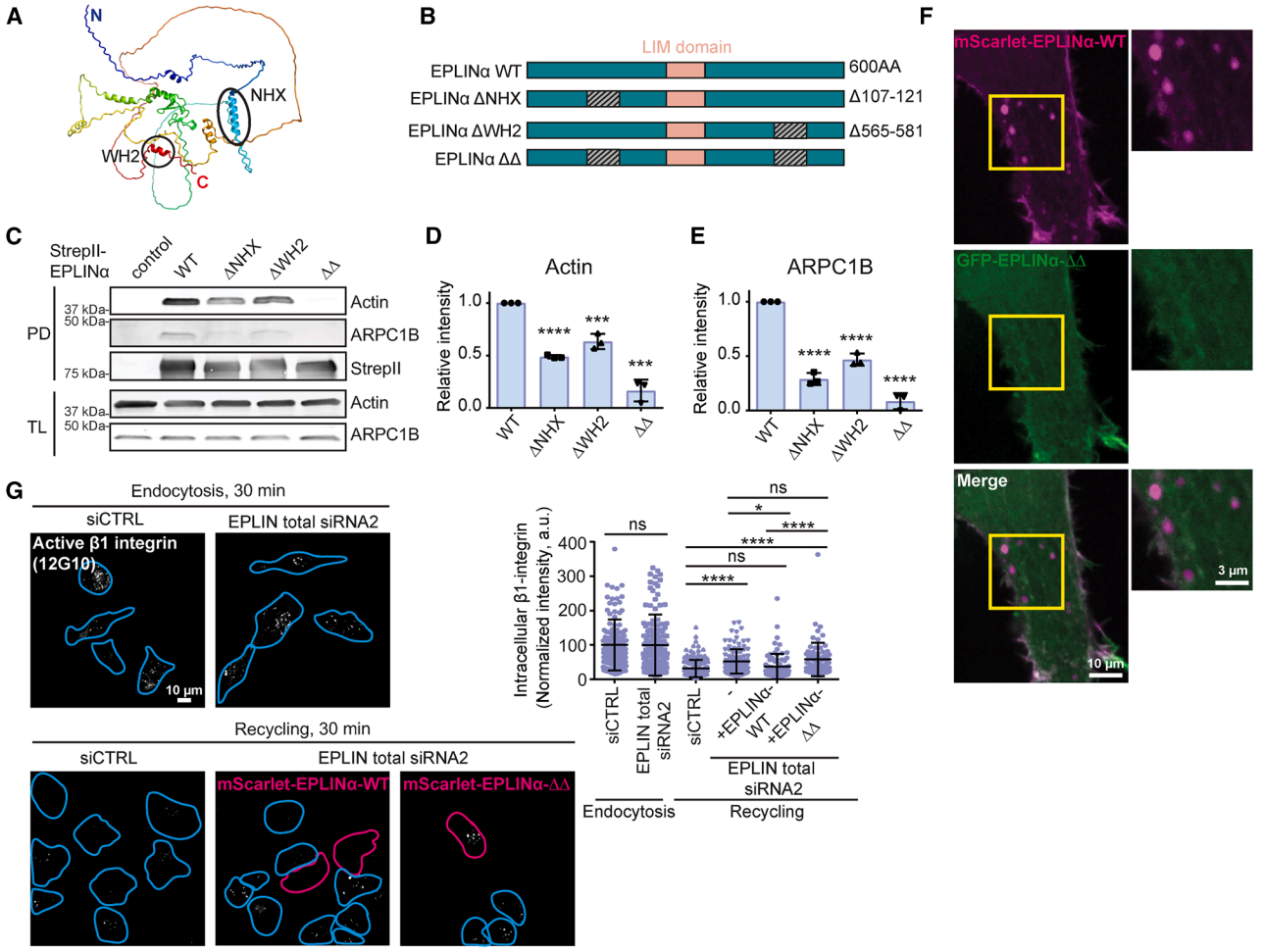

Figure 3. The actin-binding function of EPLINα is required for endosomal localization and integrin recycling

(A) AlphaFold prediction of EPLIN structure. The two actin-binding regions (N-terminal helix [NHX] and WH2 motif) are highlighted.

(B) Schematic representation of EPLINα-WT and the individual deletion mutants.

(C–E) Lysates of U2OS cells transfected with the individual StrepII-EPLINα variants were subjected to pull-down using Strep-Tactin and immunoblotted with indicated antibodies. Representative immunoblot (C) and quantification of relative amounts of actin (D) and ARPC1B (E) pulled down with individual StrepII-EPLINα variants.

(F) MDA-MB-231 live cells overexpressing mScarlet-EPLINα-WT and GFP-EPLINα-ΔΔ. ROI highlights endosomal localization of mScarlet-EPLINα-WT, but not of GFP-EPLINα-ΔΔ.

(G) Representative micrographs of internalized active β1-integrin after 30 min of endocytosis and after 30 min of recycling. Outlines of cells are shown in blue (siCTRL or EPLIN total siRNA2) and magenta (cells expressing mScarlet-EPLINα-WT or -ΔΔ). Quantification of the levels of internalized β1-integrin are shown. For endocytosis, siCTRL, $n = 151$ and EPLIN siRNA2, $n = 152$; for recycling, siCTRL, $n = 148$ and EPLIN siRNA2, $n = 105$; EPLIN siRNA2 + EPLINα-WT, $n = 78$ and EPLIN siRNA2 + EPLINα-ΔΔ, $n = 78$ cells.

Statistical significance for (D) and (E) was assessed using unpaired Student's t test and for (G) using Kruskal-Wallis one-way ANOVA and Dunn's post hoc test. $^{*}p < 0.02$, $^{***}p < 0.001$, $^{****}p < 0.0001$; ns, not significant; a.u., arbitrary units. Data shown as mean ± standard deviation. All analyzed data and representative images are from three independent experiments.

See also Figure S3 and Video S2.

(Table S1). Gene Ontology (GO) analysis of the identified proteins revealed multiple actin and cell adhesion related terms, supporting the role of EPLIN in the regulation of actin and cell adhesion[32] (Figures 4B, S4B, and S4C).

Some proximity interactors (prey) were unique to EPLIN isoforms in specific cell lines and may represent isoform- and cell-specific interactors (Figures 4C and S4D). Many of these have established roles in actin dynamics and cell migration, such as LASP1 and lamellipodin (RAPH1),[33,34] identified as EPLINα-specific interactors, and calponins CNN2 and CNN3,[35] identified as EPLINβ-specific interactors.

Comparison of the enrichment of proximity interactors of EPLINα and EPLINβ in MDA-MB-231 cells revealed that even shared proximity interactors are differentially enriched by the two isoforms (Figure 4D). This suggests that while EPLINα and EPLINβ share proximal proteins, there may be isoform-specific differences in their interactions (e.g., direct vs. indirect, duration of interaction, distance between proteins, etc.). This may also

Please cite this article in press as: Jäntti et al., EPLINα controls integrin recycling from Rab21 endosomes to drive breast cancer cell migration, Developmental Cell (2025), https://doi.org/10.1016/j.devcel.2025.06.025

CellPress
OPEN ACCESS

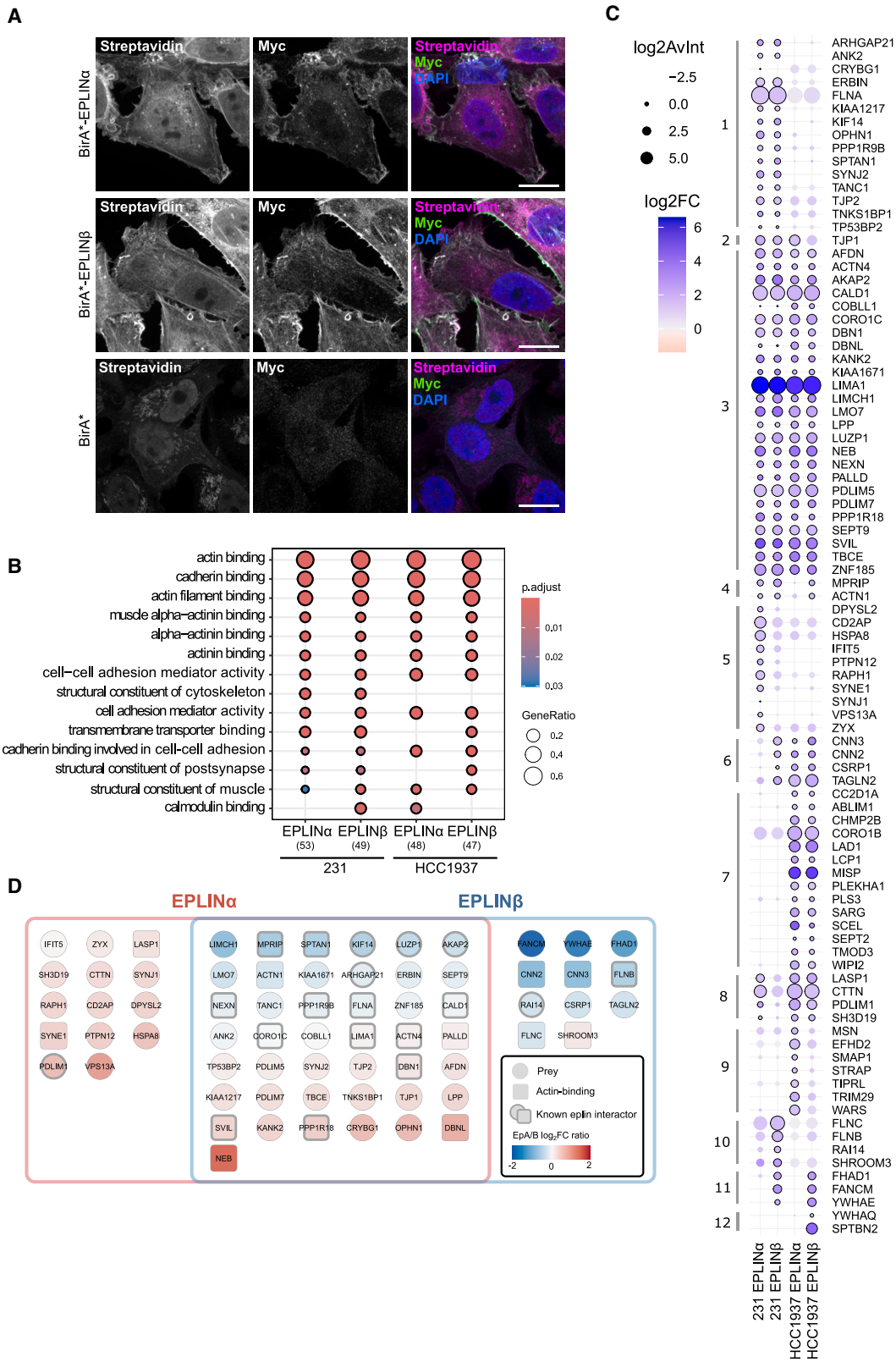

(legend on next page)

mean that, given the different localizations of the isoforms in cells, each isoform could recruit the shared interactor to a different cellular compartment.

Notable identified proximity interactors with a potential role in the regulation of endosomal traffic include supervillin 1 (SVIL), cortactin (CTTN), and CORO1C. SVIL has been shown to bind EPLIN directly, and both proteins localize to the cleavage furrow in HeLa cells.[10,36] SVIL also localizes to endosomes and promotes the recycling of β1- and β3-integrins.[37] CTTN is an activator of the Arp2/3 complex and has been implicated in the regulation of endosomal actin dynamics during cargo recycling.[38] CORO1C is an actin-binding protein that localizes to both lamellipodia and the actin cortex, as well as to actin-regulated cargo domains on endoplasmic reticulum (ER)-related endosome buds, where it enables fission of sorting endosomes.[38–41] Even though CORO1C was identified as a shared interactor of both EPLIN isoforms, we chose to focus on CORO1C, as it had not been investigated in the context of integrin recycling. Furthermore, based on the literature and our findings, CORO1C and EPLIN share a similar localization pattern in cells: CORO1C localizes to the actin cortex and lamellipodia, where both EPLIN isoforms localize, and it also localizes to endosomes, where EPLINα is the predominant isoform, prompting us to explore CORO1C in more detail.

CORO1C controls integrin recycling from Rab21- and EPLINα-positive endosomes

The initiation of the early steps of endosome fission requires the WASH complex and Arp2/3-mediated actin branching to drive membrane constriction.[42] However, recent findings suggest that halting branching nucleation by inhibiting Arp2/3 plays an important role in the later steps of fission, allowing access to other players in the fission machinery.[43] CORO1C is one Arp2/3 inhibitor implicated in this process. As EPLIN has also been shown to act as an inhibitor of Arp2/3,[21] we hypothesized that EPLINα and CORO1C could work in conjunction to facilitate the inhibition of actin branching that is needed for fission of recycling endosomes to occur. High- and super-resolution imaging revealed CORO1C localization at the cell cortex and at Rab21-positive endosomes as distinct puncta overlapping with EPLINα and F-actin (Figures 5A and 5B). Importantly, endogenous CORO1C co-precipitated with Rab21-GFP, along with endogenous EPLINα (Figure S5A), suggesting that these three proteins associate in cells. Next, we silenced CORO1C and assessed its role in integrin recycling. Loss of CORO1C led to increased intracellular β1-integrin retention after the recycling step, indicating defective recycling (Figure 5C). Since EPLIN and CORO1C are Arp2/3 inhibitors, we examined F-actin accumulation—a phenotype sometimes associated with impaired cargo recycling—on Rab21-positive endosomes in EPLIN or CORO1C-depleted cells. However, no differences were observed compared with control cells (Figure S5B). Therefore, the recycling defect is not attributed to F-actin accumulation at endosomes.

We then assessed endogenous EPLIN and CORO1C spatial proximity using a proximity ligation assay (PLA). In agreement with our immunofluorescence staining, EPLIN and CORO1C associated close to the plasma membrane, as well as in the vicinity of EEA1-positive endosomes, which was lost upon CORO1C silencing and absent in the immunoglobulin G (IgG) control (Figures 5D and S5C). Moreover, silencing Rab21 decreased the number of PLA spots specifically in the vicinity of early endosomes, but not in the entire cell, suggesting that EPLIN and CORO1C proximity on endosomes is Rab21 dependent.

Interestingly, EPLIN silencing led to a significant reduction in the cytoplasmic signal and Rab21 endosome localization of CORO1C (Figure 5E), without affecting total CORO1C protein levels (Figure 5F). In contrast, EPLIN recruitment to the endosomes was unaffected in CORO1C-silenced cells (Figure S5D), suggesting that EPLIN's endosomal localization is not CORO1C dependent. Together, these results support a model where EPLIN is recruited to early endosomes via F-actin, where it interacts with active Rab21, and the subsequent recruitment of CORO1C to this complex mediates integrin recycling.

High EPLINα expression correlates with triple-negative molecular subtype and high CORO1C expression in breast tumors

Molecular regulators of integrin intracellular transport, including Rab21 and Swip1, are overexpressed in clinical breast cancer samples, and this overexpression is linked to poorer patient prognosis.[19,44] We analyzed EPLIN expression in a cohort of 105 human breast cancer samples by immunoblotting the tumor lysates (Figure 6A). We chose this approach as the identical amino acid sequence of the two isoforms (apart from the β-specific N terminus) precludes specific detection of EPLINα with the currently available antibodies. Separating the isoforms instead by their different relative sizes, we found that the two EPLIN isoforms are expressed in different ratios among the tumors. In order to assess the contribution of each isoform to the clinical outcome,

Figure 4. Identification of the EPLINα and EPLINβ proximity interactome by BioID

(A) Immunofluorescence images of MDA-MB-231 cells stably expressing BirA*-tagged EPLINα, EPLINβ, or BirA* control. Biotin was added for 24 h to induce labeling and biotinylated proteins detected by fluorescently conjugated streptavidin. BirA*-tagged EPLIN was detected by anti-Myc antibody, and the nuclei were stained using DAPI. Scale bar, 10 μm.

(B) Gene Ontology of prey identified by BioID shows multiple enriched terms relating to actin-binding/regulation (molecular function). Number of gene names used for analysis indicated in brackets. *p*.adjust, adjusted *p* value; GeneRatio, ratio of genes identified in terms. GO analysis performed using ClusterProfiler.[30]

(C) Dotplot of high-confidence (BFDR $\leq$ 0.05) proximity interactors (prey) of BirA*-EPLINα and BirA*-EPLINβ in MDA-MB-231 and HCC1937 cells. Affinity-purified biotinylated proteins were analyzed by mass spectrometry and high-confidence (BFDR $\leq$ 0.05) interactors identified using SAINTexpress.[31] Dot size indicates the average intensity of three repeats (log_2; log2AvInt), and color indicates fold change over BirA* control (log_2; log2FC). High-confidence (BFDR $\leq$ 0.05) interactions are indicated with a black outline. Prey are organized by hierarchical clustering.

(D) Unique and shared proximity interactors (BFDR $\leq$ 0.05) identified by MDA-MB-231 cells expressing BirA*-EPLINα and BirA*-EPLINβ. Color indicates ratio between EPLINα and EPLINβ log_2 fold change over BirA* only control (EPLINα log_2 fold change/EPLINβ log_2 fold change). Square nodes indicate actin-binding proteins (UniProt annotated keywords), and thick gray borders indicate known EPLIN interactors (BioGRID).

See also Figure S4 and Table S1.

Please cite this article in press as: Jäntti et al., EPLINα controls integrin recycling from Rab21 endosomes to drive breast cancer cell migration, Developmental Cell (2025), https://doi.org/10.1016/j.devcel.2025.06.025

CellPress
OPEN ACCESS

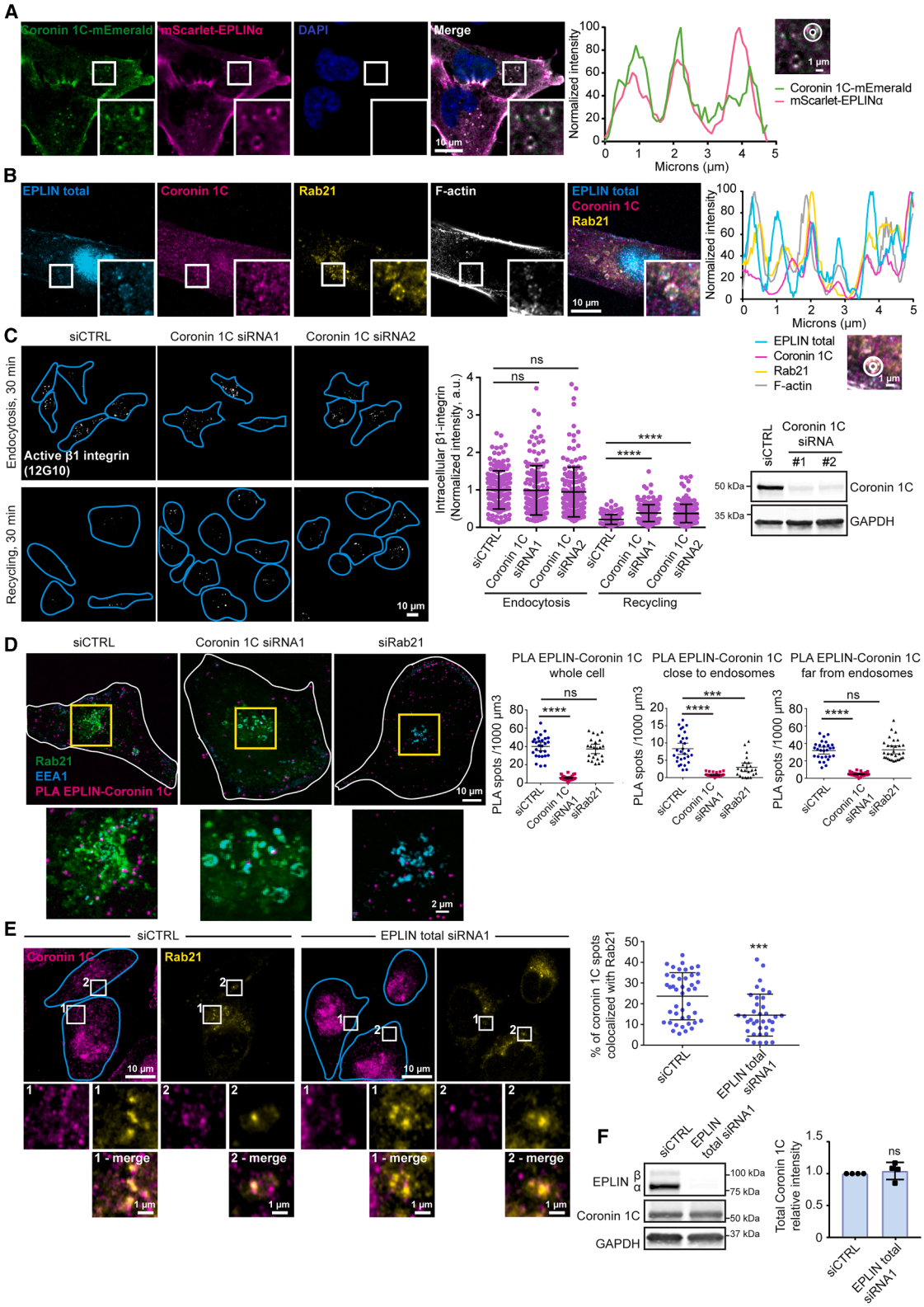

Figure 5. Coronin 1C controls integrin recycling from Rab21- and EPLINα-positive endosomes

(A) Confocal micrograph of an MDA-MB-231 cell expressing mScarlet-EPLINα and coronin 1C-mEmerald. Histogram shows fluorescence intensity at the periphery of the endosome (indicated with a circle) to show colocalization between EPLINα and coronin 1C. Cell nuclei stained with DAPI.

(legend continued on next page)

Please cite this article in press as: Jäntti et al., EPLINα controls integrin recycling from Rab21 endosomes to drive breast cancer cell migration, Developmental Cell (2025), https://doi.org/10.1016/j.devcel.2025.06.025

we categorized them into four different groups according to the expression ratio: EPLINα-high (α > β), EPLINβ-high (β > α), equal expression of both isoforms (α = β), or no EPLIN expression. Our cohort had a similar percentage of tumors in each group (Figure 6B). Many of the ER-negative tumors were EPLINα-high, and a high number of the EPLINα-high tumors belonged to the triple-negative breast cancer subtype (Figures 6C and 6D). This is interesting as our earlier work has shown that Rab21-Swip1-mediated integrin endocytosis and cell motility are linked to poor clinical outcome specifically in triple-negative breast cancer.[19] We also analyzed the disease-free survival of the patients in each EPLIN category, revealing a poorer prognosis for patients in the EPLINα-high group, although this trend did not reach statistical significance, possibly due to the relatively low number of patients (Figure 6E). Moreover, microarray data corresponding to the same breast cancer tissue cohort revealed that vimentin mRNA levels were significantly higher in the EPLINα-high group compared with the other categories, further implying a more mesenchymal phenotype for tumors with high EPLINα expression (Figure 6F). Finally, CORO1C mRNA levels were significantly higher in the EPLINα-high category compared with the other groups (Figure 6G). This is in accordance with the reported role of CORO1C in breast cancer[45] and further strengthens the role of traffic regulators, such as EPLINα and CORO1C, in triple-negative breast cancer.

Together, these findings indicate that breast tumors in which EPLINα is the predominant isoform also exhibit high CORO1C expression and are largely of the triple-negative molecular subtype. Moreover, our results suggest that the relative expression ratio of the EPLIN isoforms, rather than overall levels, correlates with the tumor phenotype and may have clinical implications in breast cancer.

EPLINα promotes cell migration and correlates with a more mesenchymal phenotype in breast cancer cells

These data prompted the hypothesis that EPLINα-high cells would display higher motility and a more mesenchymal-like phenotype compared with EPLINβ-high cells. Immunoblotting of five different breast cancer cell lines demonstrated that cell lines with high EPLINα (MDA-MD-231 and BT-549) were also characterized by high vimentin expression and loss of E-cadherin (Figure 7A), a profile associated with a mesenchymal morphology and increased cell motility and invasiveness.[46] In contrast, cell lines expressing predominantly EPLINβ (HCC1937, T47-D, and MCF7) showed high E-cadherin but no vimentin expression. This correlated with immunostaining of EPLINβ at cell-cell junctions in HCC1937 cells (Figure S6A).

Morphometric parameter analysis revealed that HCC1937, T47-D, and MCF7 have high circularity and roundness scores, whereas MDA-MD-231 and BT-549 showed a significantly more elongated morphology (Figures 7B and 7C), indicative of a less epithelial morphology.

EPLINα-high MDA-MB-231 and BT-549 cells were markedly more motile compared with the EPLINβ-high cells (Figures 7D and S6B; Video S3). Total EPLIN silencing significantly decreased MDA-MB-231 migration, which was fully rescued back to control levels by expressing GFP-EPLINα-WT. Importantly, the actin-binding-deficient mutant of EPLINα (GFP-EPLINα-ΔΔ), as well as GFP-EPLINβ-WT and GFP-EPLINβ-ΔΔ, were all unable to rescue migration speed (Figure 7E; Videos S4, S5, and S6). Thus, EPLINα supports cell migration in an actin-binding-dependent manner, presumably through its ability to support integrin recycling but possibly also through EPLINα interaction with the actin cytoskeleton.

Concordantly, CORO1C depletion significantly impeded migration (Figure 7F). Since both EPLINα and CORO1C are involved in actin dynamics, we analyzed cell morphology during random migration. Our analysis revealed no significant differences in cell area, roundness, aspect ratio, or Feret diameter between EPLIN- or CORO1C-silenced and control cells (Figures S6C and S6D). When expressed in cells, EPLINα-ΔΔ localized partially to actin protrusions at the cell cortex, thus preserving some EPLIN functionality, but was excluded from the endosomes (Figure 3F). This observation supports our hypothesis that the endosomal localization of EPLINα contributes to the migratory function of the cells.

We further investigated whether EPLIN is important for cell invasion in a more physiological matrix. We found that silencing total EPLIN reduced MDA-MB-231 cell invasion in Matrigel (Figure 7G). Overall, our results show a previously unidentified function for EPLINα and CORO1C at Rab21 endosomes, controlling integrin recycling and contributing to breast cancer cell migration and invasion.

(B) Airyscan image of an MDA-MB-231 cell expressing endogenously tagged Rab21-mScarlet and immunostained for EPLIN total and coronin 1C, and labeled with Phalloidin-Atto 647N. Histogram shows fluorescence intensity at the periphery of the endosome (indicated with a circle).
(C) Representative micrographs of internalized active β1-integrin after 30 min of endocytosis and after 30 min of recycling. Outlines of cells are shown in blue. Quantification of the levels of internalized β1-integrin are shown. For endocytosis, siCTRL, $n = 167$, coronin 1C siRNA1, $n = 158$, and siRNA2, $n = 170$; for recycling, siCTRL, $n = 167$, coronin 1C siRNA1, $n = 178$, and siRNA2, $n = 184$ cells. Cell outlines are shown in blue. Efficient silencing was validated using immunoblot.
(D) PLA assay using antibodies to detect endogenous EPLIN and coronin 1C in MDA-MB-231 cells expressing endogenously tagged Rab21-mScarlet and immunostained for EEA1. siCTRL, $n = 28$; coronin 1C siRNA1, $n = 27$; siRab21, $n = 30$ cells. Cell outlines are shown in white. Quantification of spots in the whole cell, close to EEA1 endosomes or far from EEA1 endosomes is shown.
(E) Representative images of control (siCTRL)- and EPLIN-total-silenced MDA-MB-231 cells expressing endogenously tagged Rab21-mScarlet and immunostained for coronin 1C. Coronin 1C images were quantified for colocalization with Rab21. Each dot represents the colocalization fraction in one cell. siCTRL, $n = 43$ cells; EPLIN siRNA1, $n = 37$ cells. Cell outlines are shown in blue.
(F) Immunoblot and quantification of coronin 1C expression in control (siCTRL) and EPLIN-silenced (EPLIN total siRNA1) cells. Data are plotted as the mean ± standard deviation of four independent experiments.
Statistical significance was assessed for (C) and (D) using Kruskal-Wallis one-way ANOVA, for (E) using two-sided Mann-Whitney test, and for (F) using unpaired Student's t test. $^{**}p < 0.01$, $^{***}p < 0.0006$, $^{****}p < 0.0001$; ns, not significant. Scatterplots in (C)–(E) show data as the mean ± standard deviation. All analyzed data and representative images are from three independent experiments, unless stated otherwise.
See also Figure S5.

Please cite this article in press as: Jäntti et al., EPLINα controls integrin recycling from Rab21 endosomes to drive breast cancer cell migration, Developmental Cell (2025), https://doi.org/10.1016/j.devcel.2025.06.025

CellPress
OPEN ACCESS

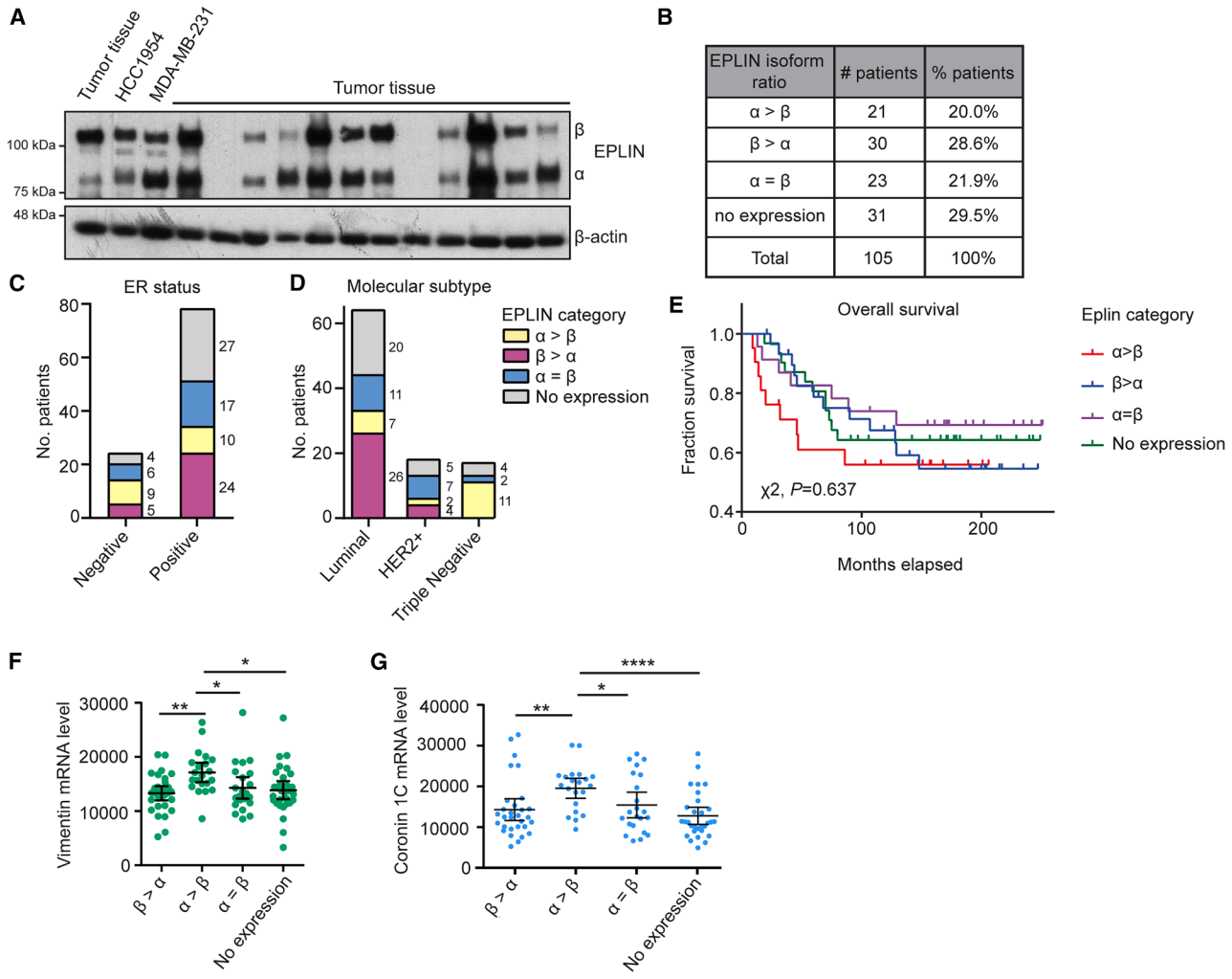

Figure 6. High expression of EPLINα correlates with triple-negative molecular subtype and high coronin 1C expression in breast tumors

(A) Representative immunoblot showing expression of EPLIN isoforms in 13 breast tumors from a cohort of 105 patients. Lysates of HCC1954 and MDA-MB-231 cells were used as controls.

(B) Tumors from 105 patients categorized into four groups: EPLIN α > β, β > α, α = β, or no expression according to the ratio of expression of EPLIN isoforms analyzed by immunoblotting. Table shows the number and percentage of tumors in each category.

(C and D) (C) ER status and (D) molecular subtype of the tumors in each EPLIN category.

(E) Kaplan-Meier plot shows overall survival of 105 patients categorized by EPLIN isoform expression. The χ^2 test was used for statistical analyses ($p = 0.637$, not significant).

(F and G) Analysis of vimentin (F) and coronin 1C (G) mRNA expression using qPCR in 105 breast tumors. Statistical significance was assessed using Kruskal-Wallis one-way ANOVA and Dunn's post hoc test, *$p < 0.04$, **$p < 0.007$, ****$p < 0.0001$. The scatter dot plots show data as the mean ± 95% CI.

DISCUSSION

Here, we report an isoform-specific function for EPLINα in breast cancer. It is the predominant EPLIN isoform in mesenchymal-type breast cancer cells, localizes to the base of tubules emanating from Rab21- and active β1-integrin-positive endosomes and positively regulates integrin recycling to support cancer cell migration and invasion.

The role of EPLIN in cancer has remained unclear, partly due to a gap in our knowledge regarding the expression pattern and function of EPLIN's individual isoforms in different tissues. Our work emphasizes the importance of this balance and its implications in cancerous and healthy tissues, and our analysis of breast tumors highlights the relevance of EPLINα in triple-negative breast cancer. Concordantly, Swip1, the cargo adaptor of Rab21-mediated integrin endocytosis, is overexpressed in tumors from this molecular subtype,[19] underlining the clinical impact of this specific active integrin transport pathway in breast cancer. Furthermore, recent work has demonstrated that EPLINα mediates migration of head and neck cancer cells,[6,7] which do not express EPLINβ. Taken together, our work identifies a role for EPLINα in the regulation of integrin trafficking and cell migration, and opens up new avenues to explore the roles of each EPLIN isoform in the context of breast cancer biology.

In our system, EPLINα is recruited to perinuclear Rab21-positive early endosomes, perhaps due to the presence of F-actin

Please cite this article in press as: Jäntti et al., EPLINα controls integrin recycling from Rab21 endosomes to drive breast cancer cell migration, Developmental Cell (2025), https://doi.org/10.1016/j.devcel.2025.06.025

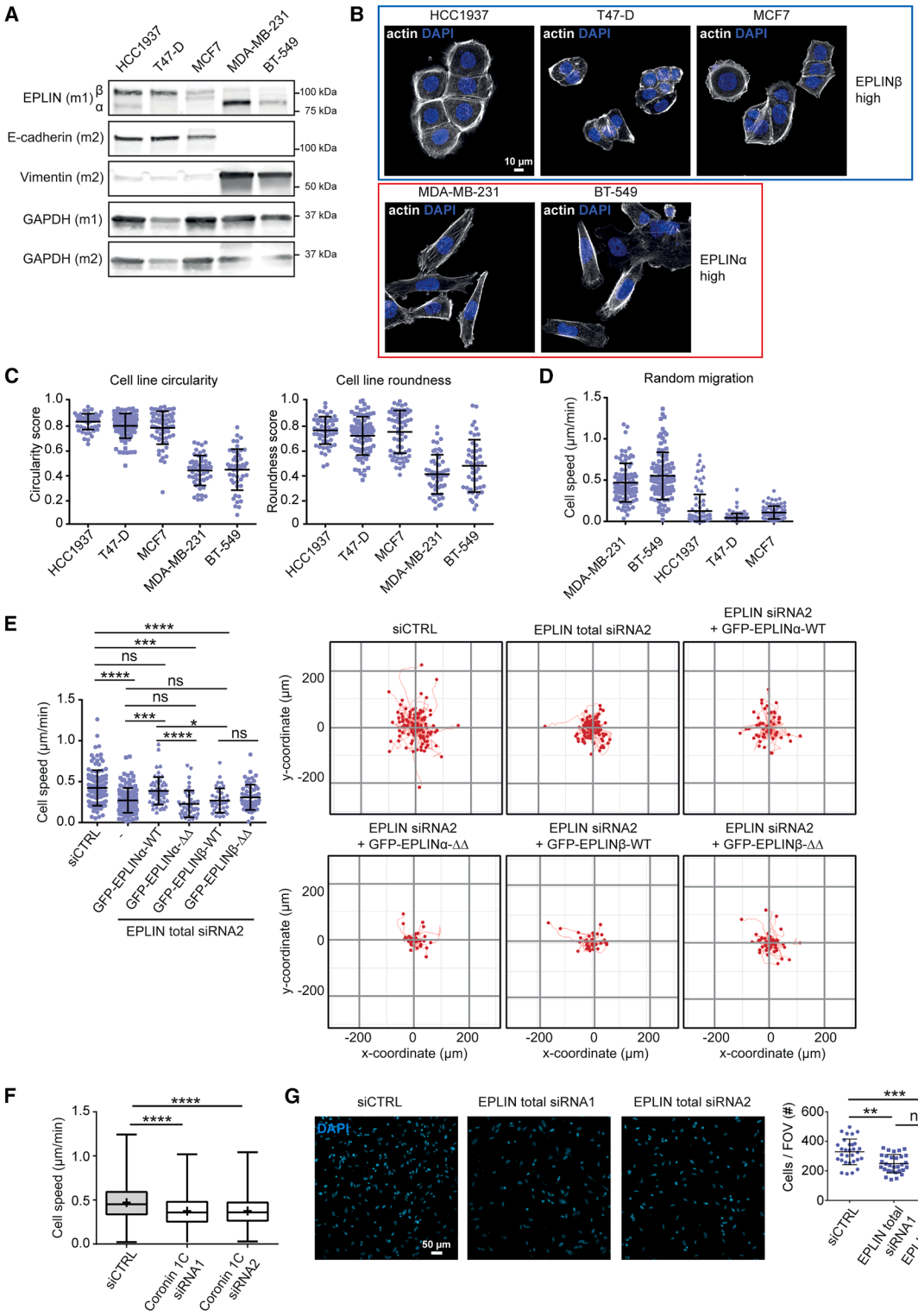

Figure 7. EPLINα promotes cell migration and correlates with a more mesenchymal phenotype in breast cancer cells

(A) Immunoblot showing expression of EPLIN isoforms, E-cadherin, and vimentin in the indicated cell lines. m1, membrane #1; m2, membrane #2.

(B) Confocal micrographs of the indicated cell lines labeled with Alexa Fluor 488 Phalloidin and DAPI.

(C) Cell circularity and cell roundness were analyzed for the indicated cell lines using Alexa Fluor 488 Phalloidin labeling to define the cell outline. HCC1937, $n = 57$; T47-D, $n = 78$; MCF7, $n = 66$; MDA-MB-231, $n = 53$; BT-549, $n = 46$ analyzed cells.

(legend continued on next page)

Please cite this article in press as: Jäntti et al., EPLINα controls integrin recycling from Rab21 endosomes to drive breast cancer cell migration, Developmental Cell (2025), https://doi.org/10.1016/j.devcel.2025.06.025

hubs in these compartments.[19] It is feasible to hypothesize that F-actin recruitment of EPLINα precedes Rab21 binding, and that complexation with Rab21 allows EPLINα to select the Rab21-associated integrin cargo for recycling. In liver hepatoma cells, EPLIN binds directly to NPC1L1 receptor at Rab11-positive endosomes, selecting it for recycling.[16,47] It would be interesting to study whether EPLIN is recruited via F-actin in this context, and whether it can control the recycling of other receptors.

F-actin is required at all steps of endocytic transport,[48–50] and the assembly of F-actin-related functional hubs at endosomes seems to be cargo specific. For example, WASH and retromer were shown to mediate the sorting of a subset of clathrin-independent cargoes, such as MCT1, SLC3A2, Basigin, and CD44 from Rab21-containing endosomes.[27] Thus, the functional hubs assembled at Rab21 endosomes are able to recognize the cargo and the fate that they need to follow. Overall, our findings ratify the crucial role that F-actin plays at Rab21-containing endosomes.

Differences in actin-binding functions have been shown for each EPLIN isoform. In endothelial cells, EPLINβ stabilizes actin bundles during shear stress, while EPLINα prevents Arp2/3-mediated actin protrusions.[21,51] This is in accordance with our findings, where EPLINα is located at membrane protrusions. At the endosomes, this function could synergize with CORO1C's inhibition of actin branching by Arp2/3 to support tubule formation.[40] Furthermore, CORO1C has been shown to interact indirectly with EHD1, a member of FERARI that mediates endosomal fission.[43] Thus, CORO1C might have a dual role at recycling endosomes, restricting actin branching and facilitating access of EHD1 to the tubulating endosomal membrane to catalyze fission. This conjecture is supported by the fact that EHD1 is required for integrin recycling.[52]

Our BioID approach reflects the observations we made across the different cell lines, where the differential functions of both EPLIN isoforms appear to occur in part due to distinct subcellular localizations. For example, some of the EPLINα-enriched interactors have a known link to endosomal transport, such as the phosphatase SYNJ1 and DPYSL2,[53,54] whereas most of the identified EPLINβ interactors have a role in stabilizing the actin cytoskeleton; calponin isoforms CNN2 and CNN3 increase stress fiber formation and resistance, while filamin B and C crosslink actin, which also confers stability to stress fibers.[35,55] In addition, SHROOM3 localizes to adherens junctions and rearranges the actin cytoskeleton to the apical side of epithelial cells.[56] The functions of the EPLINβ-specific interactors are in accordance with the more epithelial-like phenotype observed in cells where this isoform is predominantly expressed and might reflect an emerging role for EPLINβ in epithelial tissue homeostasis worth exploring in the future.

Overall, our work identifies an isoform-specific function for EPLIN, highlights its impact on integrin recycling and cell migration in breast cancer cells, and constitutes a valuable resource for exploring its emerging shared and isoform-specific functions in normal and cancer cells.

Limitations of the study

We have established that EPLINα, and not EPLINβ, mediates integrin recycling in breast cancer cells. However, in the absence of tools to specifically silence or detect EPLINα, we cannot fully evaluate the localization or the role of endogenous EPLINα. Development of new tools or strategies to specifically detect EPLINα are needed to fully elucidate the extent of EPLIN's functions in different contexts.

Our work shows that EPLINα relies on its recruitment to endosomes to promote integrin recycling. While we have perturbed endosomal EPLIN localization by mutating the actin-binding sites, this strategy does not discriminate whether the ensuing defective migration is owing to impaired actin binding or from defective recycling. Currently, we lack structural data on Rab21-EPLIN interaction, limiting the possibility to generate Rab21-binding-defective EPLINα mutants to resolve this question.

RESOURCE AVAILABILITY

Lead contact

Further information and requests for resources and reagents should be directed to and will be fulfilled by the lead contact, Johanna Ivaska (joivaska@utu.fi).

Materials availability

All unique/stable reagents generated in this study are available from the lead contact with a completed materials transfer agreement.

Data and code availability

The BioID interactome data have been deposited to the ProteomeXchange Consortium via the PRIDE partner repository with the dataset identifier "PRIDE: PXD052819". All other data that support the findings of this study are available within the paper and its supplemental information files. Any additional source data are available from the lead contact on request. This paper does not report original code.

(D) Quantification of cell velocity of the indicated cell lines migrating randomly on plastic dishes. MDA-MB-231, $n = 88$ cells; BT-549, $n = 96$ cells; HCC1937, $n = 87$ cells; T47-D, $n = 89$ cells; MCF7, $n = 74$ cells.

(E) Quantification of cell velocity in siCTRL, EPLIN total siRNA2, or EPLIN total siRNA2 together with expression of GFP-EPLINα-WT/GFP-EPLINα-ΔΔ/GFP-EPLINβ-WT/GFP-EPLINβ-ΔΔ in MDA-MB-231 cells migrating randomly on plastic dishes. siCTRL, $n = 118$ cells; EPLIN siRNA2, $n = 119$ cells; siRNA2 + GFP-EPLINα-WT, $n = 55$ cells; siRNA2 + GFP-EPLINα-ΔΔ, $n = 41$ cells; siRNA2 + GFP-EPLINβ-WT, $n = 37$ cells; siRNA2 + GFP-EPLINβ-ΔΔ, $n = 56$ cells.

(F) Quantification of cell velocity in coronin 1C-silenced MDA-MB-231 cells migrating randomly on plastic dishes. siCTRL, $n = 2{,}702$; coronin 1C siRNA1, $n = 2{,}027$; siRNA2, $n = 2{,}039$. Boxplots display the median and quartiles of the data, and the whiskers display the maxima and minima. The mean of the data is indicated with a + symbol.

(G) Matrigel invasion assays for MDA-MB-231 cells upon EPLIN total knockdown ($n = 3$, ten fields of view [FOVs] per chamber). Representative FOVs for each condition and quantification are shown.

Plots from (C)–(E) and (G) show mean ± standard deviation. Statistical significance was assessed using Kruskal-Wallis one-way ANOVA and Dunn's post hoc test. $^{****}p < 0.0001$, $^{***}p < 0.001$, $^{**}p < 0.01$, $^{*}p < 0.02$; ns, not significant. All analyzed data and representative images are from three independent experiments. See also Figure S6 and Videos S3, S4, S5, and S6.

ACKNOWLEDGMENTS

We thank P. Laasola and J. Siivonen for technical assistance and the Ivaska laboratory for critical reading of the manuscript and constructive feedback. We thank James Bear (University of North Carolina-Chapel Hill School of Medicine, Chapel Hill, North Carolina, USA) for providing reagents. The Cell Imaging and cytometry core (Turku Bioscience Centre, University of Turku and Åbo Akademi University and Biocenter Finland) are acknowledged for services, instrumentation, and expertise. We also thank Christoffer Lagerholm for assistance with image acquisition. This work was supported by the Finnish Cancer Institute (K. Albin Johansson Professorship to J.I.), a Research Council of Finland project grant (#325464 to J.I.) and Centre of Excellence program (#346131 to J.I.), the Cancer Foundation Finland (J.I.), the Sigrid Juselius Foundation (J.I.), the Research Council of Finland's Flagship InFLAMES (#337530 and 357910), the Jane and Aatos Erkko Foundation (J.I.), and European Research Council advanced grant (#101142305; Border Control). N.Z.J. was supported by the University of Turku Doctoral Programme in Technology, the Swedish Cultural Foundation in Finland, the Varsinais-Suomi Regional Fund, the K. Albin Johansson Foundation, and the Ida Montin Foundation. This study has been supported by the Research Council of Finland postdoctoral fellowships (grant nos. 321493 [to P.M.-L.], 338585 [to J.R.W.C], and 343239 [to M.R.C.]) and Research Fellowship (grant no. 360775 to J.R.W.C). J.R.W.C. was also supported by the European Union's Horizon 2020 research and innovation programme under the Marie Sklodowska-Curie grant agreement (grant 841973). M.D. was supported by the European Union's Horizon Europe research and innovation programme under Marie Sklodowska-Curie grant agreement no. 101108089.

AUTHOR CONTRIBUTIONS

Conceptualization, N.Z.J., P.M.-L., and J.I.; methodology, N.Z.J., P.M.-L., M.D., and J.I.; formal analysis and investigation, N.Z.J., P.M.-L., M.R.C., M.D., J.R.W.C., V.-M.L., K.E., L.O.-F., S.V., and J.I.; resources, S.V., L.O.-F., and K.E.; writing – original draft, N.Z.J., P.M.-L., M.R.C., M.D., J.R.W.C., and J.I.; writing – review and editing, N.Z.J., P.M.-L., M.R.C., M.D., H.H., J.R.W.C., and J.I.; visualization, N.Z.J., P.M.-L., M.R.C., M.D., H.H., and J.I.; supervision, P.M.-L. and J.I.; funding acquisition, N.Z.J., P.M.-L., and J.I.

DECLARATION OF INTERESTS

The authors declare no competing interests.

STAR★METHODS

Detailed methods are provided in the online version of this paper and include the following:

SUPPLEMENTAL INFORMATION

Supplemental information can be found online at https://doi.org/10.1016/j.devcel.2025.06.025.

Received: June 12, 2024
Revised: March 3, 2025
Accepted: June 20, 2025

REFERENCES

1. Maul, R.S., and Chang, D.D. (1999). EPLIN, epithelial protein lost in neoplasm. Oncogene *18*, 7838–7841. https://doi.org/10.1038/sj.onc.1203206.
2. Zeng, J., Jiang, W.G., and Sanders, A.J. (2021). Epithelial protein lost in neoplasm, EPLIN, the cellular and molecular prospects in cancers. Biomolecules *11*, 1038. https://doi.org/10.3390/biom11071038.
3. Wang, X., Zhang, C., Song, H., Yuan, J., Zhang, X., Yuan, Y., Zhang, L., and He, J. (2023). Characterization of LIMA1 and its emerging roles and potential therapeutic prospects in cancers. Front. Oncol. *13*, 1115943. https://doi.org/10.3389/fonc.2023.1115943.
4. Chen, S., Maul, R.S., Kim, H.R., and Chang, D.D. (2000). Characterization of the human EPLIN (epithelial protein lost in neoplasm) gene reveals distinct promoters for the two EPLIN isoforms. Gene *248*, 69–76. https://doi.org/10.1016/S0378-1119(00)00144-X.
5. Wu, D. (2017). Epithelial protein lost in neoplasm (EPLIN): Beyond a tumor suppressor. Genes Dis. *4*, 100–107. https://doi.org/10.1016/j.gendis.2017.03.002.
6. Ma, W., Liao, Y., Gao, Z., Zhu, W., Liu, J., and She, W. (2022). Overexpression of LIMA1 indicates poor prognosis and promotes epithelial-mesenchymal transition in head and neck squamous cell carcinoma. Clin. Med. Insights Oncol. *16*, 11795549221109493. https://doi.org/10.1177/11795549221109493.
7. Huang, H., Du, Y., Zhao, D., and Chen, K. (2022). The relationship between the prognostic marker LIMA1 in head and neck squamous cell carcinoma and immune infiltration. J. Oncol. *2022*, e1040116. https://doi.org/10.1155/2022/1040116.
8. Zhang, C., Wang, X., Song, H., Yuan, J., Zhang, X., Yuan, Y., Wang, Z., Lei, Z., and He, J. (2024). M6A modification-mediated LIMA1 promotes the progression of hepatocellular carcinoma through the wnt-βcatenin/Hippo pathway. Cell Biol. Toxicol. *41*, 9. https://doi.org/10.1007/s10565-024-09959-1.
9. Abe, K., and Takeichi, M. (2008). EPLIN mediates linkage of the cadherin catenin complex to F-actin and stabilizes the circumferential actin belt. Proc. Natl. Acad. Sci. USA *105*, 13–19. https://doi.org/10.1073/pnas.0710504105.
10. Chircop, M., Oakes, V., Graham, M.E., Ma, M.P.C., Smith, C.M., Robinson, P.J., and Khanna, K.K. (2009). The actin-binding and bundling protein, EPLIN, is required for cytokinesis. Cell Cycle *8*, 757–764. https://doi.org/10.4161/cc.8.5.7878.
11. Han, M.-Y., Kosako, H., Watanabe, T., and Hattori, S. (2007). Extracellular signal-regulated kinase/mitogen-activated protein kinase regulates actin organization and cell motility by phosphorylating the actin cross-linking protein EPLIN. Mol. Cell. Biol. *27*, 8190–8204. https://doi.org/10.1128/MCB.00661-07.
12. Chen, N.-P., Uddin, B., Hardt, R., Ding, W., Panic, M., Lucibello, I., Kammerer, P., Ruppert, T., and Schiebel, E. (2017). Human phosphatase CDC14A regulates actin organization through dephosphorylation of

epithelial protein lost in neoplasm. Proc. Natl. Acad. Sci. USA *114*, 5201–5206. https://doi.org/10.1073/pnas.1619356114.

13. Ohoka, A., Kajita, M., Ikenouchi, J., Yako, Y., Kitamoto, S., Kon, S., Ikegawa, M., Shimada, T., Ishikawa, S., and Fujita, Y. (2015). EPLIN is a crucial regulator for extrusion of RasV12-transformed cells. J. Cell Sci. *128*, 781–789. https://doi.org/10.1242/jcs.163113.
14. Karaköse, E., Geiger, T., Flynn, K., Lorenz-Baath, K., Zent, R., Mann, M., and Fässler, R. (2015). The focal adhesion protein PINCH-1 associates with EPLIN at integrin adhesion sites. J. Cell Sci. *128*, 1023–1033. https://doi.org/10.1242/jcs.162545.
15. Wickström, S.A., Lange, A., Montanez, E., and Fässler, R. (2010). The ILK/PINCH/parvin complex: the kinase is dead, long live the pseudokinase! EMBO J. *29*, 281–291. https://doi.org/10.1038/emboj.2009.376.
16. Zhang, Y.-Y., Fu, Z.-Y., Wei, J., Qi, W., Baituola, G., Luo, J., Meng, Y.-J., Guo, S.-Y., Yin, H., Jiang, S.-Y., et al. (2018). A LIMA1 variant promotes low plasma LDL cholesterol and decreases intestinal cholesterol absorption. Science *360*, 1087–1092. https://doi.org/10.1126/science.aao6575.
17. Paul, N.R., Jacquemet, G., and Caswell, P.T. (2015). Endocytic trafficking of integrins in cell migration. Curr. Biol. *25*, R1092–R1105. https://doi.org/10.1016/j.cub.2015.09.049.
18. Moreno-Layseca, P., Icha, J., Hamidi, H., and Ivaska, J. (2019). Integrin trafficking in cells and tissues. Nat. Cell Biol. *21*, 122–132. https://doi.org/10.1038/s41556-018-0223-z.
19. Moreno-Layseca, P., Jäntti, N.Z., Godbole, R., Sommer, C., Jacquemet, G., Al-Akhrass, H., Conway, J.R.W., Kronqvist, P., Kallionpää, R.E., Oliveira-Ferrer, L., et al. (2021). Cargo-specific recruitment in clathrin- and dynamin-independent endocytosis. Nat. Cell Biol. *23*, 1073–1084. https://doi.org/10.1038/s41556-021-00767-x.
20. Pellinen, T., Arjonen, A., Vuoriluoto, K., Kallio, K., Fransen, J.A.M., and Ivaska, J. (2006). Small GTPase Rab21 regulates cell adhesion and controls endosomal traffic of beta1-integrins. J. Cell Biol. *173*, 767–780. https://doi.org/10.1083/jcb.200509019.
21. Maul, R.S., Song, Y., Amann, K.J., Gerbin, S.C., Pollard, T.D., and Chang, D.D. (2003). EPLIN regulates actin dynamics by cross-linking and stabilizing filaments. J. Cell Biol. *160*, 399–407. https://doi.org/10.1083/jcb.200212057.
22. Linklater, E.S., Duncan, E.D., Han, K.-J., Kaupinis, A., Valius, M., Lyons, T. R., and Prekeris, R. (2021). Rab40-Cullin5 complex regulates EPLIN and actin cytoskeleton dynamics during cell migration. J. Cell Biol. *220*, e202008060. https://doi.org/10.1083/jcb.202008060.
23. Alanko, J., Mai, A., Jacquemet, G., Schauer, K., Kaukonen, R., Saari, M., Goud, B., and Ivaska, J. (2015). Integrin endosomal signalling suppresses anoikis. Nat. Cell Biol. *17*, 1412–1421. https://doi.org/10.1038/ncb3250.
24. Croucher, D.R., Iconomou, M., Hastings, J.F., Kennedy, S.P., Han, J.Z.R., Shearer, R.F., McKenna, J., Wan, A., Lau, J., Aparicio, S., et al. (2016). Bimolecular complementation affinity purification (BiCAP) reveals dimer-specific protein interactions for ERBB2 dimers. Sci. Signal. *9*, ra69. https://doi.org/10.1126/scisignal.aaf0793.
25. Mai, A., Veltel, S., Pellinen, T., Padzik, A., Coffey, E., Marjomäki, V., and Ivaska, J. (2011). Competitive binding of Rab21 and p120RasGAP to integrins regulates receptor traffic and migration. J. Cell Biol. *194*, 291–306. https://doi.org/10.1083/jcb.201012126.
26. Grant, B.D., and Donaldson, J.G. (2009). Pathways and mechanisms of endocytic recycling. Nat. Rev. Mol. Cell Biol. *10*, 597–608. https://doi.org/10.1038/nrm2755.
27. Del Olmo, T., Lauzier, A., Normandin, C., Larcher, R., Lecours, M., Jean, D., Lessard, L., Steinberg, F., Boisvert, F.-M., and Jean, S. (2019). APEX2-mediated RAB proximity labeling identifies a role for RAB21 in clathrin-independent cargo sorting. EMBO Rep. *20*, e47192. https://doi.org/10.15252/embr.201847192.
28. Sönnichsen, B., De Renzis, S., Nielsen, E., Rietdorf, J., and Zerial, M. (2000). Distinct membrane domains on endosomes in the recycling pathway visualized by multicolor imaging of Rab4, Rab5, and Rab11. J. Cell Biol. *149*, 901–914. https://doi.org/10.1083/jcb.149.4.901.
29. Abramson, J., Adler, J., Dunger, J., Evans, R., Green, T., Pritzel, A., Ronneberger, O., Willmore, L., Ballard, A.J., Bambrick, J., et al. (2024). Accurate structure prediction of biomolecular interactions with AlphaFold 3. Nature *630*, 493–500. https://doi.org/10.1038/s41586-024-07487-w.
30. Wu, T., Hu, E., Xu, S., Chen, M., Guo, P., Dai, Z., Feng, T., Zhou, L., Tang, W., Zhan, L., et al. (2021). clusterProfiler 4.0: A universal enrichment tool for interpreting omics data. Innovation (Camb.) *2*, 100141. https://doi.org/10.1016/j.xinn.2021.100141.
31. Teo, G., Liu, G., Zhang, J., Nesvizhskii, A.I., Gingras, A.-C., and Choi, H. (2014). SAINTexpress: improvements and additional features in Significance Analysis of INTeractome software. J. Proteomics *100*, 37–43. https://doi.org/10.1016/j.jprot.2013.10.023.
32. Collins, R.J., Jiang, W.G., Hargest, R., Mason, M.D., and Sanders, A.J. (2015). EPLIN: a fundamental actin regulator in cancer metastasis? Cancer Metastasis Rev. *34*, 753–764. https://doi.org/10.1007/s10555-015-9595-8.
33. Law, A.-L., Vehlow, A., Kotini, M., Dodgson, L., Soong, D., Theveneau, E., Bodo, C., Taylor, E., Navarro, C., Perera, U., et al. (2013). Lamellipodin and the Scar/WAVE complex cooperate to promote cell migration in vivo. J. Cell Biol. *203*, 673–689. https://doi.org/10.1083/jcb.201304051.
34. Lin, Y.H., Park, Z.-Y., Lin, D., Brahmbhatt, A.A., Rio, M.-C., Yates, J.R., and Klemke, R.L. (2004). Regulation of cell migration and survival by focal adhesion targeting of Lasp-1. J. Cell Biol. *165*, 421–432. https://doi.org/10.1083/jcb.200311045.
35. Liu, R., and Jin, J.P. (2016). Calponin isoforms *CNN*1, *CNN*2 and *CNN*3: Regulators for actin cytoskeleton functions in smooth muscle and non-muscle cells. Gene *585*, 143–153. https://doi.org/10.1016/j.gene.2016.02.040.
36. Smith, T.C., Fang, Z., and Luna, E.J. (2010). Novel interactors and a role for supervillin in early cytokinesis. Cytoskeleton (Hoboken) *67*, 346–364. https://doi.org/10.1002/cm.20449.
37. Fang, Z., Takizawa, N., Wilson, K.A., Smith, T.C., Delprato, A., Davidson, M.W., Lambright, D.G., and Luna, E.J. (2010). The membrane-associated protein, supervillin, accelerates F-actin-dependent rapid integrin recycling and cell motility. Traffic *11*, 782–799. https://doi.org/10.1111/j.1600-0854.2010.01062.x.
38. Puthenveedu, M.A., Lauffer, B., Temkin, P., Vistein, R., Carlton, P., Thorn, K., Taunton, J., Weiner, O.D., Parton, R.G., and von Zastrow, M. (2010). Sequence-dependent sorting of recycling proteins by actin-stabilized endosomal microdomains. Cell *143*, 761–773. https://doi.org/10.1016/j.cell.2010.10.003.
39. Hoyer, M.J., Chitwood, P.J., Ebmeier, C.C., Striepen, J.F., Qi, R.Z., Old, W.M., and Voeltz, G.K. (2018). A novel class of ER membrane proteins regulates ER-associated endosome fission. Cell *175*, 254–265.e14. https://doi.org/10.1016/j.cell.2018.08.030.
40. Striepen, J.F., and Voeltz, G.K. (2022). Coronin 1C restricts endosomal branched actin to organize ER contact and endosome fission. J. Cell Biol. *221*, e202110089. https://doi.org/10.1083/jcb.202110089.
41. King, Z.T., Butler, M.T., Hockenberry, M.A., Subramanian, B.C., Siesser, P. F., Graham, D.M., Legant, W.R., and Bear, J.E. (2022). Coro1B and Coro1C regulate lamellipodia dynamics and cell motility by tuning branched actin turnover. J. Cell Biol. *221*, e202111126. https://doi.org/10.1083/jcb.202111126.
42. Duleh, S.N., and Welch, M.D. (2010). WASH and the Arp2/3 complex regulate endosome shape and trafficking. Cytoskeleton (Hoboken) *67*, 193–206. https://doi.org/10.1002/cm.20437.
43. Dhawan, K., Naslavsky, N., and Caplan, S. (2022). Coronin2A links actin-based endosomal processes to the EHD1 fission machinery. Mol. Biol. Cell *33*, ar107. https://doi.org/10.1091/mbc.E21-12-0624.
44. Ye, F., Tang, H., Liu, Q., Xie, X., Wu, M., Liu, X., Chen, B., and Xie, X. (2014). miR-200b as a prognostic factor in breast cancer targets multiple members of RAB family. J. Transl. Med. *12*, 17. https://doi.org/10.1186/1479-5876-12-17.

45. Castagnino, A., Castro-Castro, A., Irondelle, M., Guichard, A., Lodillinsky, C., Fuhrmann, L., Vacher, S., Agüera-González, S., Zagryazhskaya-Masson, A., Romao, M., et al. (2018). Coronin 1C promotes triple-negative breast cancer invasiveness through regulation of MT1-MMP traffic and invadopodia function. Oncogene *37*, 6425–6441. https://doi.org/10.1038/s41388-018-0422-x.

46. Dongre, A., and Weinberg, R.A. (2019). New insights into the mechanisms of epithelial–mesenchymal transition and implications for cancer. Nat. Rev. Mol. Cell Biol. *20*, 69–84. https://doi.org/10.1038/s41580-018-0080-4.

47. Xiao, J., Dong, L.-W., Liu, S., Meng, F.-H., Xie, C., Lu, X.-Y., Zhang, W.J., Luo, J., and Song, B.-L. (2023). Bile acids-mediated intracellular cholesterol transport promotes intestinal cholesterol absorption and NPC1L1 recycling. Nat. Commun. *14*, 6469. https://doi.org/10.1038/s41467-023-42179-5.

48. Chakrabarti, R., Lee, M., and Higgs, H.N. (2021). Multiple roles for actin in secretory and endocytic pathways. Curr. Biol. *31*, R603–R618. https://doi.org/10.1016/j.cub.2021.03.038.

49. McNally, K.E., and Cullen, P.J. (2018). Endosomal retrieval of cargo: retromer is not alone. Trends Cell Biol. *28*, 807–822. https://doi.org/10.1016/j.tcb.2018.06.005.

50. Zech, T., Calaminus, S.D.J., and Machesky, L.M. (2012). Actin on trafficking: could actin guide directed receptor transport? Cell Adh. Migr. *6*, 476–481. https://doi.org/10.4161/cam.21373.

51. Taha, M., Aldirawi, M., März, S., Seebach, J., Odenthal-Schnittler, M., Bondareva, O., Bojovic, V., Schmandra, T., Wirth, B., Mietkowska, M., et al. (2019). EPLIN-α and -β isoforms modulate endothelial cell dynamics through a spatiotemporally differentiated interaction with actin. Cell Rep. *29*, 1010–1026.e6. https://doi.org/10.1016/j.celrep.2019.09.043.

52. Jović, M., Naslavsky, N., Rapaport, D., Horowitz, M., and Caplan, S. (2007). EHD1 regulates β1 integrin endosomal transport: effects on focal adhesions, cell spreading and migration. J. Cell Sci. *120*, 802–814. https://doi.org/10.1242/jcs.03383.

53. Rahajeng, J., Giridharan, S.S.P., Naslavsky, N., and Caplan, S. (2010). Collapsin response mediator protein-2 (Crmp2) regulates trafficking by linking endocytic regulatory proteins to dynein motors. J. Biol. Chem. *285*, 31918–31922. https://doi.org/10.1074/jbc.C110.166066.

54. Fasano, D., Parisi, S., Pierantoni, G.M., De Rosa, A., Picillo, M., Amodio, G., Pellecchia, M.T., Barone, P., Moltedo, O., Bonifati, V., et al. (2018). Alteration of endosomal trafficking is associated with early-onset parkinsonism caused by SYNJ1 mutations. Cell Death Dis. *9*, 385. https://doi.org/10.1038/s41419-018-0410-7.

55. Stossel, T.P., Condeelis, J., Cooley, L., Hartwig, J.H., Noegel, A., Schleicher, M., and Shapiro, S.S. (2001). Filamins as integrators of cell mechanics and signalling. Nat. Rev. Mol. Cell Biol. *2*, 138–145. https://doi.org/10.1038/35052082.

56. Hildebrand, J.D. (2005). Shroom regulates epithelial cell shape via the apical positioning of an actomyosin network. J. Cell Sci. *118*, 5191–5203. https://doi.org/10.1242/jcs.02626.

57. Chastney, M.R., Lawless, C., Humphries, J.D., Warwood, S., Jones, M.C., Knight, D., Jorgensen, C., and Humphries, M.J. (2020). Topological features of integrin adhesion complexes revealed by multiplexed proximity biotinylation. J. Cell Biol. *219*, e202003038. https://doi.org/10.1083/jcb.202003038.

58. Pedley, R., King, L.E., Mallikarjun, V., Wang, P., Swift, J., Brennan, K., and Gilmore, A.P. (2020). BioID-based proteomic analysis of the Bid interactome identifies novel proteins involved in cell-cycle-dependent apoptotic priming. Cell Death Dis. *11*, 872. https://doi.org/10.1038/s41419-020-03091-8.

59. Vennin, C., Chin, V.T., Warren, S.C., Lucas, M.C., Herrmann, D., Magenau, A., Melenec, P., Walters, S.N., Del Monte-Nieto, G., Conway, J.R.W., et al. (2017). Transient tissue priming via ROCK inhibition uncouples pancreatic cancer progression, sensitivity to chemotherapy, and metastasis. Sci. Transl. Med. *9*, eaai8504. https://doi.org/10.1126/scitranslmed.aai8504.

60. Zhang, J.-P., Li, X.-L., Li, G.-H., Chen, W., Arakaki, C., Botimer, G.D., Baylink, D., Zhang, L., Wen, W., Fu, Y.-W., et al. (2017). Efficient precise knockin with a double cut HDR donor after CRISPR/Cas9-mediated double-stranded DNA cleavage. Genome Biol. *18*, 35. https://doi.org/10.1186/s13059-017-1164-8.

61. Yusa, K., Zhou, L., Li, M.A., Bradley, A., and Craig, N.L. (2011). A hyperactive piggyBac transposase for mammalian applications. Proc. Natl. Acad. Sci. USA *108*, 1531–1536. https://doi.org/10.1073/pnas.1008322108.

62. Chastney, M.R., Lawless, C., and Humphries, M.J. (2020). Multiplexed proximity biotinylation coupled to mass spectrometry for defining integrin adhesion complexes. Curr. Protoc. Cell Biol. *88*, e113. https://doi.org/10.1002/cpcb.113.

63. Roux, K.J., Kim, D.I., Raida, M., and Burke, B. (2012). A promiscuous biotin ligase fusion protein identifies proximal and interacting proteins in mammalian cells. J. Cell Biol. *196*, 801–810. https://doi.org/10.1083/jcb.201112098.

64. Roux, K.J., Kim, D.I., and Burke, B. (2013). BioID: a screen for protein-protein interactions. Curr. Protoc. Protein Sci. *91*, 19–23. https://doi.org/10.1002/0471140864.ps1923s74.

65. Cox, J., and Mann, M. (2008). MaxQuant enables high peptide identification rates, individualized p.p.b.-range mass accuracies and proteome-wide protein quantification. Nat. Biotechnol. *26*, 1367–1372. https://doi.org/10.1038/nbt.1511.

66. Tyanova, S., Temu, T., and Cox, J. (2016). The MaxQuant computational platform for mass spectrometry-based shotgun proteomics. Nat. Protoc. *11*, 2301–2319. https://doi.org/10.1038/nprot.2016.136.

67. UniProt Consortium (2023). UniProt: the Universal Protein Knowledgebase in 2023. Nucleic Acids Res. *51*, D523–D531. https://doi.org/10.1093/nar/gkac1052.

68. Perez-Riverol, Y., Csordas, A., Bai, J., Bernal-Llinares, M., Hewapathirana, S., Kundu, D.J., Inuganti, A., Griss, J., Mayer, G., Eisenacher, M., et al. (2019). The PRIDE database and related tools and resources in 2019: improving support for quantification data. Nucleic Acids Res. *47*, D442–D450. https://doi.org/10.1093/nar/gky1106.

69. Shannon, P., Markiel, A., Ozier, O., Baliga, N.S., Wang, J.T., Ramage, D., Amin, N., Schwikowski, B., and Ideker, T. (2003). Cytoscape: a software environment for integrated models of biomolecular interaction networks. Genome Res. *13*, 2498–2504. https://doi.org/10.1101/gr.1239303.

70. Szklarczyk, D., Kirsch, R., Koutrouli, M., Nastou, K., Mehryary, F., Hachilif, R., Gable, A.L., Fang, T., Doncheva, N.T., Pyysalo, S., et al. (2023). The STRING database in 2023: protein–protein association networks and functional enrichment analyses for any sequenced genome of interest. Nucleic Acids Res. *51*, D638–D646. https://doi.org/10.1093/nar/gkac1000.

71. Oughtred, R., Rust, J., Chang, C., Breitkreutz, B.J., Stark, C., Willems, A., Boucher, L., Leung, G., Kolas, N., Zhang, F., et al. (2021). The BioGRID database: A comprehensive biomedical resource of curated protein, genetic, and chemical interactions. Protein Sci. *30*, 187–200. https://doi.org/10.1002/pro.3978.

72. von Chamier, L., Laine, R.F., Jukkala, J., Spahn, C., Krentzel, D., Nehme, E., Lerche, M., Hernández-Pérez, S., Mattila, P.K., Karinou, E., et al. (2021). Democratising deep learning for microscopy with ZeroCostDL4Mic. Nat. Commun. *12*, 2276. https://doi.org/10.1038/s41467-021-22518-0.

73. Schmidt, U., Weigert, M., Broaddus, C., and Myers, G. (2018). Cell Detection with Star-Convex Polygons. In Medical Image Computing and Computer Assisted Intervention—MICCAI 2018, A.F. Frangi, J.A. Schnabel, C. Davatzikos, C. Alberola-López, and G. Fichtinger, eds. (Springer International Publishing), pp. 265–273. https://doi.org/10.1007/978-3-030-00934-2_30.

74. Milde-Langosch, K., Karn, T., Schmidt, M., zu Eulenburg, C., Oliveira-Ferrer, L., Wirtz, R.M., Schumacher, U., Witzel, I., Schütze, D., and Müller, V. (2014). Prognostic relevance of glycosylation-associated genes in breast cancer. Breast Cancer Res. Treat. *145*, 295–305. https://doi.org/10.1007/s10549-014-2949-z.

Please cite this article in press as: Jäntti et al., EPLINα controls integrin recycling from Rab21 endosomes to drive breast cancer cell migration, Developmental Cell (2025), https://doi.org/10.1016/j.devcel.2025.06.025

STAR★METHODS

KEY RESOURCES TABLE

REAGENT or RESOURCE	SOURCE	IDENTIFIER
Antibodies		
Rabbit anti-EPLIN antibody	Novus	Cat# NB100-2305; RRID: AB_2136662
Mouse anti-EPLIN β antibody	Invitrogen	Cat# MA5-27016; RRID: AB_2724255
Mouse anti-GAPDH antibody	HyTest	Cat# 5G4cc; RRID: AB_2858176
Mouse anti-integrin β1 (12G10) antibody	Supernatant from hybridoma provided by K.M. Yamada (NIH, Bethesda, MD)	N/A
Alexa Fluor488 mouse anti-integrin β1 (12G10-488) antibody	Abcam	Cat# ab202641
Mouse anti-β-actin antibody	Sigma-Aldrich	Cat# A1978; RRID: AB_476692
Mouse anti-StrepII-tag antibody	Novus	Cat# NBP2-43735; RRID: AB_2916323
Rabbit anti-Arp2/3 subunit 1B antibody	Abcam	Cat# ab99314; RRID: AB_10675894
Rabbit anti-Alexa488 antibody	Invitrogen	Cat# 710369
Mouse anti-myc-tag (9B11) antibody	Cell signaling technology	Cat# 2276S; RRID: AB_331783
Mouse anti-CORO1C antibody	Generated in-house by J.E. Bear (University of North Carolina-Chapel Hill School of Medicine, Chapel Hill, NC).	N/A
Rabbit anti-E-cadherin (24E10) antibody	Cell signaling technology	Cat# 3195; RRID: AB_2291471
Mouse anti-vimentin (V9) antibody	Santa Cruz Biotechnology	Cat# sc-6260; RRID: AB_628437
Mouse anti-β-actin antibody (patient sample loading control)	Santa Cruz Biotechnology	Cat# sc-47778; RRID: AB_626632
Rabbit anti-CORO1C antibody	Proteintech	Cat#14749-1-AP; RRID: AB_2230110
Rabbit anti-Rab5 antibody (C8B1)	Cell signaling technology	Cat# 3547; RRID: AB_2300649
Rabbit anti-EEA1 antibody (C45B10)	Cell signaling technology	Cat# 3288; RRID: AB_2096811
Mouse IgG isotype control	Invitrogen	Cat# 02-6502; RRID: AB_2532951
Biological samples		
Breast cancer patient samples	University Medical Center Hamburg Eppendorf, Germany. Milde-Langosch et al.[74]	N/A
Chemicals, peptides, and recombinant proteins		
Rab21 GppNHp (GTP analogue)	Moreno-Layseca et al.[19]	N/A
Rab21 GDP	Moreno-Layseca et al.[19]	N/A
GST-EPLINα	This paper	N/A
Critical commercial assays		
Duolink Proximity Ligation Assay kit	Sigma-Aldrich	DUO92013
Deposited data		
EPLIN BioID interactome data	ProteomeXchange Consortium via PRIDE	PRIDE: PXD052819
Experimental models: Cell lines		
MDA-MB-231	American Type Culture Collection ATCC	HTB-26
BT-549	American Type Culture Collection ATCC	HTB-122
HCC1937	American Type Culture Collection ATCC	CRL-2336
T-47D	American Type Culture Collection ATCC	HTB-133
MCF7	American Type Culture Collection ATCC	HTB-22
U2OS	Leibniz Institute DSMZ-German Collection of Microorganisms and Cell Cultures	ACC 785
MDA-MB-231 Rab21 endogenously tagged with mScarlet	This paper	N/A

(*Continued on next page*)

Please cite this article in press as: Jäntti et al., EPLINα controls integrin recycling from Rab21 endosomes to drive breast cancer cell migration, Developmental Cell (2025), https://doi.org/10.1016/j.devcel.2025.06.025

Continued

REAGENT or RESOURCE	SOURCE	IDENTIFIER
Oligonucleotides		
See Table S2 for a list of siRNAs and primers	N/A	N/A
Recombinant DNA		
pEGFP-EPLINα	Addgene	40947
pEGFP-EPLINβ	Addgene	40948
pmScarlet-EPLINα	This paper	N/A
pmScarlet-EPLINβ	This paper	N/A
pPB-TagBFP-T2A-myc-BirA*	This paper	N/A
pPB-TagBFP-T2A-myc-BirA*-EPLINα	This paper	N/A
pPB-TagBFP-T2A-myc-BirA*-EPLINβ	This paper	N/A
pDEST-V2-EPLINα	This paper	N/A
pDEST-Rab21-V1	Moreno-Layseca et al.[19]	N/A
pRab21-GFP	Addgene	83421
pLL5.0-hCORO1C-mEmerald	From J.E. Bear (University of North Carolina-Chapel Hill School of Medicine, Chapel Hill, NC).	N/A
pEGFP-EPLINα-ΔΔ	This paper	N/A
pEGFP-EPLINβ-ΔΔ	This paper	N/A
pmScarlet-EPLINα-ΔΔ	This paper	N/A
pmScarlet-EPLINβ-ΔΔ	This paper	N/A
StrepII-EPLINα	This paper	N/A
StrepII-EPLINα-ΔΔ	This paper	N/A
pXPR_001-sgRAB21	This paper	N/A
pUC57-RAB21 HDR	This paper	N/A
Software and algorithms		
Fiji	National Institutes of Health	https://imagej.net/software/fiji/
Imaris (v.10.2.0)	Oxford Instruments	https://imaris.oxinst.com/
Huygens Professional (v.24.04)	Scientific Volume Imaging	https://svi.nl/Huygens-Professional
MaxQuant (v.2.0.3.0)	Max Planck Institute of Biochemistry	https://www.maxquant.org/
ZeroCostDL4Mic	Von Chamier et al.[72]	https://github.com/HenriquesLab/ZeroCostDL4Mic
SPSS (v.23)	IBM	https://www.ibm.com/products/spss-statistics
Prism 7	Graphpad	https://www.graphpad.com/
RStudio (v.4.2.2)	Posit	https://posit.co/download/rstudio-desktop/
MO Affinity Analysis (v.1.6)	Nanotemper	https://shop.nanotempertech.com/en/moaffinity-analysis-software-unlimited-licenses-34

EXPERIMENTAL MODEL AND STUDY PARTICIPANT DETAILS

Cell lines and culture conditions

The human breast cancer cell lines MDA-MB-231, BT-549, HCC1937, T-47D and MCF7 were purchased from American Type Culture Collection (ATCC; cat. numbers in order: HTB-26, HTB-122, CRL-2336, HTB-133 and HTB-22). MDA-MB-231 cells were cultured in Dulbecco's Modified Eagle's Medium (DMEM) (VWR, 392-0413) supplemented with 10 % fetal bovine serum (Sigma, F7524), 2 mM L-glutamine (Sigma-Aldrich, G7513-100ML) and 1x non-essential amino acids (Sigma-Aldrich, M7145-100ML). BT-549 cells were cultured in RPMI-1640 medium (VWR, 392-0429) supplemented with 10 % fetal bovine serum (Sigma-Aldrich, F7524), 2 mM L-glutamine (Sigma-Aldrich, G7513-100ML) and 0.023 U/ml human insulin (Sigma-Aldrich, I9278-5ML). HCC1937 cells were cultured in RPMI-1640 medium (VWR, 392-0429) supplemented with 10 % fetal bovine serum (Sigma-Aldrich, F7524) and 2 mM L-glutamine (Sigma-Aldrich, G7513-100ML). T-47D cells were cultured in RPMI-1640 medium (VWR, 392-0429) supplemented with 10 % fetal bovine serum (Sigma-Aldrich, F7524), 2 mM L-glutamine (Sigma-Aldrich, G7513-100ML) and 0.2 U/ml human insulin (Sigma-Aldrich, I9278-5ML). MCF7 cells were cultured in DMEM (VWR, 392-0413) supplemented with 10 % fetal bovine

serum (Sigma-Aldrich, F7524), 2 mM L-glutamine (Sigma-Aldrich, G7513-100ML) and 0.01 mg/ml human insulin (Sigma-Aldrich, I9278-5ML). U2OS cells were purchased from Leibniz Institute DSMZ-German Collection of Microorganisms and Cell Cultures and cultured in Dulbecco's Modified Eagle's Medium (DMEM) (VWR, 392-0413) supplemented with 10 % fetal bovine serum (Sigma, F7524) and 2 mM L-glutamine (Sigma-Aldrich, G7513-100ML). The cells were routinely tested for mycoplasma contamination and cultured at 37°C, 5% CO_2 in a humidified incubator.

METHOD DETAILS

Transfection

The expression of proteins of interest was suppressed transiently using Lipofectamine RNAiMAX reagent (Thermo Fisher Scientific, 56532) according to the manufacturer's instructions. The siRNAs were transfected at a concentration of 30 nM per oligo. The siRNA oligonucleotides targeting human *LIMA1*/EPLIN were purchased from Horizon Discovery: EPLIN total siRNA1 (Accell A-010663-14, sequence GGCUUAAGAUGAUGUUUGA), EPLIN total siRNA2 (ON-TARGETplus J010633-09-0002, GCUUAAACAUUACGACUGA) and EPLINβ siRNA1 (Dharmacon_A010663-13, UCACUAUCAUUGAGGGUAA). EPLINβ siRNA2 was designed using the online tool BLOCK-iT™ RNAi Designer and custom-made from Invitrogen, (CAGGUAUUUCAGUGUCUGUAGACAA). The siRNA oligonucleotides targeting human CORO1C/coronin 1C were purchased from Horizon Discovery: CORO1C siRNA1 (ON-TARGETplus J017331-05-0002) and CORO1C siRNA2 (ON-TARGETplus J017331-06-0002). The siRNA used as control (siCTRL) was Allstars negative control siRNA (Qiagen, cat. no. 1027281). Plasmids of interest were transfected using Lipofectamine 3000 (Invitrogen, 100022052) according to the manufacturer's instructions.

Plasmids

GFP-EPLINα and GFP-EPLINβ were obtained from Addgene (plasmids 40947 and 40948, respectively). To generate the mScarlet-I-tagged EPLINα, PCR was first performed using pEFHD2-mScarlet-I as a template for mScarlet-I with the mScarlet_F GATCCG CTAGCGCTACCGGTCGCCACCATGGTGAGCA and mScarlet_R GGATCTGAGTCCGGACTTGTACAGCTCGTCCATGCC primers. Overlap extension PCR was then performed for EPLINα using the pEGFP-EPLINα (Addgene plasmid 40947) as template and the EPLIN_F ACGAGCTGTACAAGTCCGGACTCAGA and EPLIN_R CCGGTGGATCCCGGGC primers. The overlapped fragments were then digested with NheI/KpnI (New England Biosciences) restriction enzymes and ligated into the similarly digested pEGFP-EPLINα backbone using T4 DNA Ligase (ThermoFisher, EL0011). All plasmids were validated by analytical digests and sequencing.

In order to generate the BioID constructs, the entry vectors pENTR2B-EPLINα and pENTR2B-EPLINβ were first generated using HiFi DNA assembly according to the manufacturer's instructions (New England Biolabs). The primer sequences used to make the plasmids are listed in Table S2. Vectors were linearised using restriction enzymes indicated for 1 hour at 37°C. PCR-amplified inserts and linearised vectors were purified (and sizes confirmed) using gel extraction. To generate pPB-TagBFP-T2A-myc-BirA* (pPB-BirA*), TagBFP-T2A-myc-BirA* was amplified from pCDH-TagBFP-myc-BirA*[57,58] and inserted into a pPB destination vector, pPB-DEST,[59] linearized by BspDI and XhoI. To generate EPLINα and EPLINβ BioID plasmids (pPB-TagBFP-T2A-myc-BirA*-EPLINα and pPB-TagBFP-T2A-myc-BirA*-EPLINβ; herein referred to as BirA*-EPLINα and BirA*-EPLINβ, respectively), full length EPLIN ORFs (Addgene plasmids 40947 and 40948) were amplified by PCR and inserted into the pPB-TagBFP-T2A-myc-BirA* vector that was linearized using BspDI and XhoI. For pENTR2B-EPLINα, full length EPLIN ORFs were amplified by PCR and inserted into the pENTR2B vector (Gateway pENTR 2B Dual Selection Vector, Invitrogen) linearized by SalI and EcoRV restriction enzymes. pDEST_V2-EPLINα was generated by gateway cloning. Using LR Clonase II (Invitrogen), pENTR2B-EPLINα was LR subcloned with a pDEST-V2-ORF (Addgene 73636) according the manufacturers' protocol. Sequences were confirmed using DNA sequencing.

pLL5.0-hCORO1C-mEmerald was a gift from James Bear (University of North Carolina-Chapel Hill School of Medicine, Chapel Hill, North Carolina, USA).

StrepII-EPLINα WT plasmid was created by inserting the EPLINα PCR product (created with EPLINα Strep F/R primers) into pcDNA3 StrepII MCS vector cleaved with *EcoRI*/*AgeI* using NEBuilder HiFi DNA Assembly (NEB). The deletion mutants (ΔNHX, ΔWH2) were created using whole plasmid synthesis approach using the primers specified in Table S2. Briefly, after PCR with the indicated primers and StrepII-EPLINα WT pcDNA3 as a template, the reaction was cleaned using KAPA Pure Beads (Roche), digested with *DpnI* and transformed into DH5α *E. coli* strain. The actin binding-deficient mutant StrepII-EPLINα ΔΔ pcDNA3 was generated introducing the ΔNHX mutation into StrepII-EPLINα ΔWH2 pcDNA3 plasmid. The mScarlet-I/GFP EPLINα mutant constructs were generated as above using mScarlet-I/GFP EPLINα WT as template. All the constructs were verified by sequencing.

Endogenous tagging of Rab21

MDA-MB-231 cells expressing endogenously tagged Rab21 were generated using homology-directed repair-mediated (HDR) CRISPR/Cas9 targeting Exon 1 of Rab21-201 transcript (Transcript ID ENST00000261263.5). Corresponding guide sequence (AGC GACGGGATGGCTGCGGC) was cloned into pXPR_001 lentiCRISPR v1 plasmid (Addgene #49535) cleaved with BsmBI (NEB). Final construct (pXPR_001-sgRAB21) was verified by sequencing. The template for HDR was designed based on Zhang et al.[60] and synthesized into pUC57 mini plasmid (final plasmid pUC57-RAB21 HDR; GenScript). The sequence of mScarlet-I, followed by a short linker, was surrounded by approximately 850 bp-long homology arms and flanked with Rab21 Cas9 guide sequence to generate double-cut dsDNA donor sequence for recombination. MDA-MB-231 cells were co-transfected with pXPR_001-sgRab21 and pUC57-Rab21 HDR plasmids in 1:4 ratio using Lipofectamine 3000 (Invitrogen). Five days post-transfection, the cells were sorted

Please cite this article in press as: Jäntti et al., EPLINα controls integrin recycling from Rab21 endosomes to drive breast cancer cell migration, Developmental Cell (2025), https://doi.org/10.1016/j.devcel.2025.06.025

using Sony SH800S Cell Sorter for red fluorescence, expanded, and resorted again to obtain the cell population with the highest fluorescence intensity.

Western Blotting

Cells were washed with cold PBS and scraped into a TX lysis buffer (TXLB; 50 mM Tris-HCl, pH 7.5, 150 mM NaCl, 0.5% Triton-X, 0.5% glycerol, 1% SDS, Complete protease inhibitor (Sigma-Aldrich, 5056489001), and phos-stop tablet (Sigma-Aldrich, 49068 37001). SDS sample buffer was added to the lysates, samples were placed on a heat block (+90 °C) for 10 minutes and separated by SDS–polyacrylamide gel electrophoresis (4–20% Mini-PROTEAN TGX gels, Bio-Rad, 456-1096). Proteins were transferred to a nitrocellulose membrane (Bio-Rad, #1704159) using the Trans-Blot Turbo transfer system (Bio-Rad) and the membrane was blocked with StartingBlock blocking buffer (Thermo Fisher Scientific, 37538) for 1 hour at room temperature. Primary antibodies against proteins of interest were added to the membrane and the membrane was incubated with the antibody solution overnight at +4 °C, followed by incubation with fluorophore-conjugated secondary antibodies for 1 hour at room temperature. All antibodies were diluted in StartingBlock blocking buffer (Thermo Fisher Scientific, 37538). Membranes were scanned with the Odyssey infrared imaging system (LI-COR Biosciences).

BiFC microscopy

Cells plated on 6-well plates were co-transfected with split Venus constructs pDEST-V2-EPLINα and pDEST-Rab21-V1.[19] The next morning, the transfected cells were detached using trypsin, and plated on glass-bottom dishes (Cellvis, D35-14-1.5-N). Samples were fixed 5 hours after plating with warm 4% paraformaldehyde for 15 minutes. The above-mentioned steps for immunofluorescence staining were then followed. The samples were imaged with a 3i (Intelligent Imaging Innovations, 3i Inc) Marianas spinning disk confocal microscope, Hamamatsu ORCA-Flash4.0 v2 scientific complementary metal-oxide semiconductor (sCMOS) camera (Hamamatsu Photonics), and Plan-Apochromat 63x, 1.4 NA oil objective.

Migration assay

Cells were plated on a 6-well plate in full growth medium. Before imaging, medium was changed to full growth medium containing 25 mM HEPES. Cells were imaged every 10 or 20 minutes for 6 hours at +37 °C and 5% CO_2 using a Nikon Eclipse Ti-E epifluorescence microscope and Plan Fluor 10x, 0.30 NA objective (Nikon), controlled by NIS-Elements AR 4.60 software (Nikon). To quantify cell migration, single migrating cells were tracked with the MTrackJ plug-in for Fiji (ImageJ, National Institutes of Health). Cells were tracked based on phase contrast signal or, in the case of cells expressing a plasmid construct, based on fluorescent protein signal. Dividing or dying cells were excluded from the analysis. RStudio (Posit) was used to plot migration tracks.

Immunofluorescence staining and microscopy

Cells plated on glass-bottom dishes (Cellvis, D35-14-1.5-N or Mattek, P35G-0.170-14-C) were fixed with 2% paraformaldehyde for 15 minutes, permeabilized for 15 minutes with 0.3% Triton X-100 in 10% horse serum (Gibco, 16050-122) in PBS and blocked for 20 minutes with 10% horse serum in PBS. Samples were incubated with primary antibodies diluted in 10% horse serum overnight at +4 °C. Secondary antibodies were diluted in 10% horse serum and the samples were incubated with the secondary antibodies for 1-2 hours at room temperature. Where indicated, cell nuclei were stained using DAPI and filamentous actin with Phalloidin-Atto 647N (Sigma-Aldrich, 65906), Alexa Fluor 488 Phalloidin (Invitrogen, A12379) or SiR-actin (Spirochrome, SC001).

For SIM and Airyscan imaging, cells plated on glass-bottom dishes (MatTek, P35G-0.170-14-C) were fixed with 4% paraformaldehyde for 15 minutes and treated as described above, with an additional post-fixation step (4 % paraformaldehyde, 10 min) after incubation with secondary antibodies and Phalloidin-Atto 647N.

Structured illumination microscopy (SIM) was performed using a DeltaVision OMX v4 (GE Healthcare Life Sciences) with a front-illuminated pco.edge sCMOS camera (pixel size 6.5 mm, readout speed 95 MHz; PCO AG) and a Plan-Apochromat 60x, 1.42 NA objective (immersion oil RI of 1.516). SIM illumination mode (five phases x three rotations) was used, and the microscope was controlled by SoftWorx.

Airyscan imaging was performed using a LSM880 laser scanning confocal microscope (Zeiss) equipped with an Airyscan detector and 63x oil, NA 1.4 objective. Standard super-resolution mode was used for Airyscan imaging, and the microscope was controlled with Zen Black (2.3).

Live imaging of tubulating endosomes was performed using a Leica Stellaris 8 Falcon FLIM microscope equipped with a Plan APO 63x 1.40 NA oil immersion objective. Acquisition was done for 252 frames every 0.66 seconds using a pinhole setting of 1AU at 580 nm with unidirectional scanning with the resonance scanner at a line speed of 8kHz. Detection was done in photon counting mode with a line accumulation of 10 lines. Image channels were in Track 1, simultaneous excitation at 487 nm and 650 nm with detection windows at 488-530 nm (HyD X detector) and 658-717 nm (HyD X detector), and in Track 2 excitation at 569 nm and emission window of 582-640 nm (HyD S detector).

Integrin internalization assay

Cells on Cellvis glass-bottom dishes were placed in +4 °C to cool down for 15 minutes, after which they were incubated on ice with primary antibody against active β1-integrin (12G10) diluted in cold full growth medium for 1 hour to label cell surface integrins. Samples were washed twice with cold full growth medium, and warm full growth medium was added before placing the samples in an

incubator at +37 °C to allow antibody-labeled integrin internalization for 15 minutes. Internalization was then stopped by changing to cold medium, and samples were placed on ice. Samples were washed twice with an acid wash solution (0.2 M acetic acid and 0.5 M NaCl, pH 2.5) to remove the remaining antibodies from the cell surface. Finally, samples were fixed with 2% paraformaldehyde for 20 minutes at room temperature. Quantification of internalized integrins was performed on 3D projections of the cells using the cell wizard to detect cell body and vesicles of different size (region growing) in IMARIS software (Oxford Instruments, v.10.2.0). The intensity sum of all of the vesicles in a cell was divided by the cell's volume. All intensity values were then normalized to the average of the control condition (siCTRL).

Integrin recycling assay

Cells were starved for 45 minutes in warm serum-free medium at +37 °C, after which samples were cooled down at +4 °C for 10 minutes before fluorophore-conjugated 12G10 (12G10 conjugated to Alexa 488, 12G10-488), diluted in cold serum-free medium, was added to the samples and incubated for 1 hour on ice to label cell surface integrins. Samples were washed twice with cold serum-free medium, after which warm serum-free medium was added before placing the samples in an incubator at +37 °C to allow antibody-labeled integrin endocytosis for 30 minutes. Endocytosis was then stopped by adding cold serum-free medium and placing samples on ice. Next, an anti-Alexa 488 antibody, diluted in cold serum-free medium (50 μg/ml), was added to the samples and incubated for 1 hour on ice. The anti-Alexa 488 antibody binds to 12G10-488-bound integrins, effectively quenching the fluorescent signal from the integrins left on the cell surface. To start integrin recycling, warm full growth medium containing the anti-Alexa 488 quenching antibody was added to the samples and incubated at +37 °C for 30 minutes. As 12G10-488-bound integrins are recycled from inside the cell and reach the cell surface, their fluorescence is effectively extinguished by the quenching antibody in the medium. Finally, samples were fixed with 2% paraformaldehyde for 20 minutes at room temperature. Samples were stained with Phalloidin-Atto 647N (see above) and imaged with a 3i (Intelligent Imaging Innovations, 3i Inc) Marianas spinning disk confocal microscope with a Yokogawa CSU-W1 scanner and a back-illuminated 10 MHz EMCDD camera (Photometrics Evolve) with a 63x/1.4 oil objective. Intracellular integrin signal intensity per cell, normalized to cell area, was quantified using Fiji (ImageJ, National Institutes of Health) using mean background-subtracted sum projections of 21 slices from the middle of the cell.

Microscale thermophoresis

For microscale thermophoresis (MST), GppNHp-loaded Rab21[19] was labeled using amine-reactive NT-650-NHS fluorescent dye (Nanotemper) using 1:2 protein:dye concentration ratio. Excess dye was removed by centrifugation using centrifugal filters (Millipore). GST-tagged EPLINα was expressed in *E. coli* and purified as described elsewhere. Protein concentrations were determined using Bradford assay (Bio-Rad). Binding experiments were carried out in 10 mM HEPES, pH 7.4, 150 mM NaCl, 5 mM $MgCl_2$, 0.05% Tween-20. The binding assays were performed using a fixed concentration (50 nM) of the fluorescently labeled Rab21(target) and two-fold serially diluted decreasing concentrations of the unlabeled EPLINα (ligand). 12 serial dilutions of the ligand and labelled protein were loaded into the standard capillaries (Nanotemper, MO-K022) and analyzed using the Monolith NT.Automated instrument. All experiments were carried out at RT using a medium MST power. Normalization of the fluorescence signal and fitting to the KD equation were performed using the software MO Affinity Analysis v1.6 (Nanotemper). Recombinant Rab21 was purified and loaded with either GDP or GppNHp as previously reported.[19]

Endosome line scan analysis

For line scan analyses of endosomes, a single-plane image from the middle of the endosome was used. A circular, clockwise free-hand line was drawn around the endosome, after which intensity values of the different channels were measured, normalized to values between 0-100, and plotted as a function of length.

Colocalization analysis

Analysis of colocalization using Pearson's coefficients was performed with the Coloc2 plug-in for Fiji (ImageJ, National Institutes of Health). Spot co-localization analysis was performed in Z stacks of the cells using the plugin ComDet in ImageJ (https://imagej.net/Spots_colocalization_comdet), with a pixel size >5 and pixel distance, 4. The ratio of co-localization was calculated as a percentage of co-localized spots per cell.

Deconvolution

Where indicated, AiryScan images were deconvolved using Huygens Professional version 24.04 (Scientific Volume Imaging). Raw data were analyzed using Array Detector Quality Control tool and deconvolved using CMLE algorithm with 15 iterations and the recommended settings.

BioID and affinity purification of proteins

For stable expression of pPB-BioID constructs (BirA*, BirA*-EPLINα and BirA*-EPLINβ) in 231 and HCC1957 cells, pPB-BioID constructs were co-transfected with a plasmid containing the piggyBac transposase, pCMV hypBase,[61] with a 3 to 1 ratio (pPB-BioID vector: pCMV-HypBase) using Lipofectamine 3000 according to manufacturers' instructions. Fresh media was added to cells the following day. Cells were passaged for two weeks before being FACs sorted for BFP expression to select high- and low-expressing cells. Cell populations were selected based on expression levels and subcellular targeting of BirA*-tagged proteins, aiming for equal

Please cite this article in press as: Jäntti et al., EPLINα controls integrin recycling from Rab21 endosomes to drive breast cancer cell migration, Developmental Cell (2025), https://doi.org/10.1016/j.devcel.2025.06.025

levels of expression and efficient subcellular targeting. Although the low-expressing BirA*-EPLINα and BirA*-EPLINβ and high-expressing BirA* control cells were selected, BirA* expression levels were significantly lower.

For biotinylation of proximal proteins, cells were seeded onto 10 cm dishes (two per condition) one day before the addition of biotin (from 20X solution in media, final concentration of 50 μM) to induce biotinylation. After 24h incubation with biotin, cells were lysed and biotinylated proteins affinity-purified following a previously described BioID protocol[57,62] adapted from Roux et al.[63,64] At RT, cells were washed 3 x with 10 ml PBS before 400 μl cell lysis buffer added (250 mM NaCl, 50 mM Tris HCl (pH 7.4), 0.1 % SDS (w/v), 0.5 mM DTT and 1X protease inhibitors (cOmplete Mini, EDTA-free, Roche). Cells were scraped, and lysates (~800 μl per condition) added to 80 μl 20% (v/v) Triton X-100. From herein, lysates were kept at 4°C. Lysates were passed four times through a 19G needle before 720 μl 50 mM Tris HCl (pH 7.4) added. Lysates were then passed through a 27G needed a further 4 times, before centrifugation for 10 m at full speed at 4°C. The supernatant was incubated with 30 μl MagReSyn magnetic streptavidin beads (ReSyn Biosciences; washed twice with lysis buffer) overnight at 4°C, with rotation. The following day, the beads were washed with multiple stringent buffers (500 μl each, 5 min) to remove non-specific proteins: twice with wash buffer 1 (10% SDS (w/v)), followed by one wash each of wash buffer 2 (500 mM NaCl, 50 mM HEPES, 1 mM EDTA, 1% Triton X-100 (w/v), 0.1% deoxycholic acid (w/v)) and wash buffer 3 (10 mM Tris HCl (pH 7.4), 1 mM EDTA, 0.5 % NP-40 (w/v), 0.5% deoxycholic acid (w/v)). To elute proteins, beads were incubated with 90 μl 2X reducing sample buffer with 10 μM biotin at 70°C for ten minutes. Western blotting confirmed the presence of biotinylated proteins before the samples prepared for label free quantitative mass spectrometry (MS).

MS sample preparation

Samples were prepared for MS using in-gel trypsin digestion. Samples were subjected to SDS-PAGE for 4 minutes (or until all the sample had entered the gel) at 200V (two wells per sample; 4-20% Mini-PROTEAN TGX precast protein gel, BIO-RAD), then stained with Coomassie blue for ten minutes before being washed 4 X with ddH_2O (10 minutes each, with a final wash overnight at 4°C). Protein bands were excised and gel pieces were washed twice with 0.04 M NH_4HCO_3/50% acetonitrile (ACN) for 15 mins, before incubation with 100% ACN for 10 mins. Proteins were reduced with 20 mM DL-Dithiothreitol (DTT; BioUltra, for molecular biology, Sigma) at 56°C for 30 minutes, followed by addition of 100% ACN for 10 mins, and proteins alkylated with 55 mM iodoacetamide (Sigma) in 100 mM NH_4HCO_3 for 20 mins at RT (protected from light). Gel pieces were washed twice with 100 mM NH_4HCO_3 and dehydrated with 100% ACN followed by centrifugation in a vacuum centrifuge. Proteins were digested using 0.005 μg/μl trypsin (sequencing grade modified trypsin; Promega) in 40 mM NH_4HCO_3/10% ACN at 4°C for 20 minutes followed by 16 h at 37°C. Peptides were extracted by incubating with 100% ACN followed by 50% ACN/5% formic acid (Thermo Fisher) for 15 mins each at 37°C. The supernatant was collected after each step of peptide extraction, and dried in a vacuum centrifuge. Peptides were dissolved in 10 μl 2% formic acid immediately prior to MS analysis.

MS data acquisition

Samples were analyzed by liquid chromatography-electrospray ionization-tandem mass spectrometry (LC-ESI-MS/MS) using a nanoflow HPLC system (Easy-nLC1200, Thermo Fisher Scientific) coupled to a Q Exactive HF mass spectrometer (Thermo Fisher Scientific, Bremen, Germany) equipped with a nano-electrospray ionization source. Peptides were first loaded on a trapping column and subsequently separated inline on a 15 cm C18 column (75 μm x 15 cm, ReproSilPur 3 μm 120 Å C18-AQ, Dr. Maisch HPLC GmbH, Ammerbuch-Entringen, Germany). The mobile phase consisted of water with 0.1% formic acid (solvent A) and ACN/water (80:20; v/v) with 0.1% formic acid (solvent B). To elute peptides, a 30 min linear gradient from 6% to 39% of solvent B was used, followed by a wash stage with 100% eluent B. MS data were automatically acquired using Thermo Xcalibur 4.1 software (Thermo Fisher Scientific). Data dependent acquisition was used, consisting of repeated cycles of a single MS1 scan covering a range of m/z 350–1750 plus a series of HCD fragment ion scans (MS2 scans) for up to 10 of the highest intensity peptide ions from the MS1 scan.

MaxQuant processing and bioinformatics

MS data were processed and bioinformatic analyses performed as described previously.[57,62] Raw MS data were analyzed using MaxQuant (v2.0.3.0, available from Max Planck Institute of Biochemistry)[65,66] using default parameters, with biotinylation of lysines as a variable modification and selecting match between runs, LFQ quantification, and unique peptides only for quantification. Experiments were searched against the human proteome (UniProtKB/Swiss-Prot[67] accessed April 2023). The BioID interactome data has been deposited to the ProteomeXchange Consortium via the PRIDE[68] partner repository with the dataset identifier ''PRIDE: PXD052819''. SAINTexpress[31] (via REPRINT; https://reprint-apms.org/) was used to identify high-confidence bait-prey interactions using LFQ intensities from MaxQuant, using default parameters and MS1-based processing. A BFDR of $\leq$ 0.05 was used as a threshold to identify bait-prey interactions considered as proximal interactors. Dotplots were generated using R and prey organized by hierarchical clustering (Jaccard distance). Prey groups were assigned numbers (1–12) to aid identification of prey. Gene ontology analysis was performed using ClusterProfiler (version 4.8.3).[30] Interactome networks were generated using Cytoscape, version 3.10.1.[69] Actin-binding proteins were identified using UniProt Annotated Keywords via STRING.[70] 'Known EPLIN interactors' were those identified from BioGRID, accessed February 2024.[71]

Proximity Ligation Assay (PLA)

MDA-MB-231 cells growing on coverslips were fixed, washed twice with PBS and permeabilized with 0.3% Triton X-100 in PBS for 15 min at room temperature. The cells were stained using mouse anti-coronin 1C antibody (1.2:100) and rabbit anti-EPLIN (1:100)

primary antibodies diluted in 5% horse serum for 1 h at room temperature. Proximity ligation was performed according to the manufacturer's instructions (Duolink in situ PLA, Sigma-Aldrich), followed by immunostaining using an anti-EEA1 antibody previously conjugated to CoraLite 647 with the FlexAble CoraLite Plus 647 Antibody Labeling Kit for Rabbit IgG (Proteintech, KFA503). Cells were imaged with a confocal 3i (Intelligent Imaging Innovations, 3i Inc) Marianas spinning disk microscope with a ×100/1.4 oil objective. The number of PLA spots between EPLIN and coronin 1C per 1,000 μm3 inside and outside the endosomes was determined using the IMARIS software (Oxford Instruments, v.10.2.0). The cell wizard for vesicle detection was used to determine cell volume and number of spots per cell. Then, the EEA1 endosomal signal was segmented as a surface and the PLA spots close to the surface were classified with the "Spots close to surface" XTension using a threshold value of 1μm.

Cell morphology analyses

Cell circularity and roundness of MDA-MD-231, BT-549, HCC1937, T47-D and MCF7 cells were analyzed using Fiji (ImageJ, National Institutes of Health). Cell outlines were drawn based on F-actin staining, and circularity and roundness were selected as measurement parameters from Fiji's built-in shape descriptors function before performing the measurement. Cell morphology parameters of EPLIN- or coronin 1C-silenced and control MDA-MB-231 cells were analyzed in five fields of view from each condition of the random migration experiments. Segmentation of the cells was performed using CellPose, via ZCDL4Mic Google colab notebooks.[72] Cell masks were generated using the following settings: model: cytoplasm3, diameter: 50, flow threshold: 0.4 and mask threshold: 0. Masks were manually adjusted and then analyzed for their area, Feret diameter, aspect ratio and roundness.

Matrigel Invasion Assay

Total EPLIN-silenced cells or control cells (2×10^5 cells per chamber in 500 μl serum-free medium) were seeded onto Matrigel invasion chambers (354480, Corning). The bottom chamber was then filled with 1 ml of serum-containing medium. The cells were allowed to invade for 6 hours at 37°C and then fixed with 4% PFA in PBS. The remaining cells at the top chamber were removed with a cotton swab and then the cells were stained with DAPI before imaging on a spinning disk confocal microscope (3i Marianas CSU-W1; 20×/0.45 objective). The number of invading cells were quantified from ten fields per condition in ImageJ using StarDist2D.[73]

Breast tumor sample analysis

The breast cancer patient cohort has been previously described in Milde-Langosch et al.[74] Briefly, tumor samples were obtained from 105 primary breast cancer patients treated at the University Medical Center Hamburg Eppendorf, Germany, Department of Gynecology between 1991-2002. All tissue samples were snap-frozen after surgery and stored in liquid nitrogen until use. From those samples, vimentin and coronin 1C mRNA levels were analyzed using microarray data (Affymetrix, Santa Clara, CA, USA) after RNA extraction and statistical analyses were conducted using SPSS software Version 23 (SPSS Inc., Chicago, IL, USA).

Protein extracts from the same samples were obtained by lysing tumor fragments with RIPA buffer to analyze EPLIN isoforms expression. Tumor lysates were subjected to SDS-PAGE followed by protein transfer and immunoblotting with primary antibodies (anti EPLIN, Novus Cat# NB100-2305 and anti β-actin, Santa Cruz Cat# sc-47778). Signal amplification was performed with HRP-conjugated secondary antibodies (Goat Anti Mouse IgG and Anti Rabbit IgG from Southern Biotech, #130-05 1:8000, Lot: E2518-Z909), diluted 1:8,000 in blocking buffer, at room temperature for 1 h. The membranes were developed and expression of each EPLIN isoform was quantified using ImageJ. The ratio between both isoforms was calculated (EPLINβ/EPLINα). The cohort was then divided into four groups according to the ratio of EPLIN isoforms (cutoff values: Group β>α, ratio >1.3, Group α>β, ratio <0.7, Group α=β, ratio between 0.7 and 1.3) and the clinicopathological factors (ER status and molecular subtype) of each sample correlated and plotted as the number of patients.

QUANTIFICATION AND STATISTICAL ANALYSIS

Statistical analyses and plotting of data were performed using Prism 7 (GraphPad). *P value*s and statistical tests used are indicated in the figure legends. $P < 0.05$ was considered significant. Data are presented as mean ± SD of three independent experiments unless stated otherwise in the figure legends.